

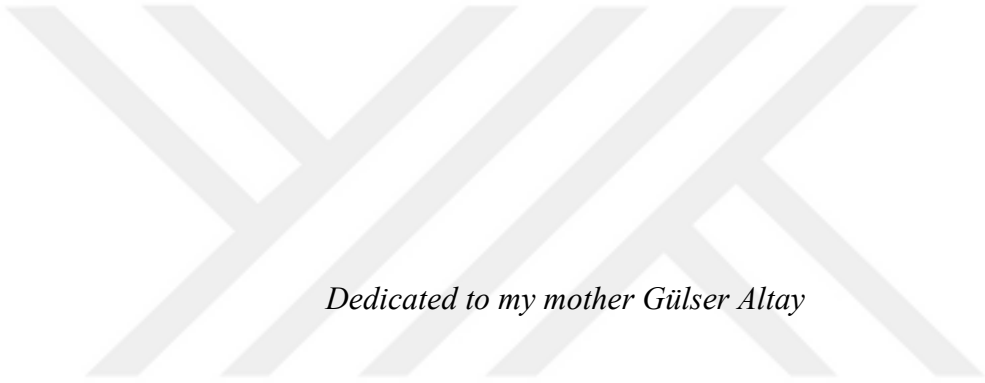
**DEVELOPMENT OF REAL TIME BLOOD VESSEL
IMAGING SYSTEM FOR EARLY DIAGNOSIS OF
VASCULAR DISEASES**

**A Thesis Submitted to
the Graduate School of Engineering and Sciences of
İzmir Institute of Technology
in Partial Fulfillment of the Requirements for the Degree of
MASTER OF SCIENCE**

in Electronics and Communication Engineering

**by
Ayşe ALTAY**

**November 2020
İZMİR**



Dedicated to my mother Gülser Altay

ACKNOWLEDGMENTS

It wouldn't have been possible to write this Master's thesis without the help and support of certain people whom I would like to give particular acknowledge here. Their contributions are sincerely appreciated.

I would first like to thank my thesis advisor Assist. Prof. Dr. Abdurrahman Gümüş for his encouragement, his guidance, his mentorship and his persistent help throughout my thesis study. Dr. Gümüş has shared his knowledge, and put in effort at all times during my graduate studies. I have learned so much from his advices.

I would like to express my deepest appreciation to my dissertation committee members, Assist. Prof. Dr. M. Zübeyir Ünlü and Prof. Dr. Aydın Akan for taking their time out of their busy schedule and to provide me with advice and guidance on my thesis.

I would like to thank Assoc. Prof. Dr. Şevket Gümüştekin for allowing me to use his laboratory resources for 3D modeling of the device.

I would also like to thank to all my professors who has been invaluable on both academic and personal level throughout my education in Electrical and Electronics Engineering Master's program at Izmir Institute of Technology.

I would like to thank you to Izmir Institute of Technology for their support in this project by Scientific Research Projects Coordination Unit (BAP) 2020IYTE0112.

I would like to express special thanks to the volunteers who participated in my research for their help as their contribution was so important to my research.

Thanks to all of my friends, especially Selin Bozburun, Deniz Doğan and Hüseyin Selman Aşık for their never-ending support and friendship.

Last but not least, I am deeply thankful to my family, my parents, Gülser Altay and İlhan Altay, and my siblings, Ebru, Esra, Tuba and Büşra for their continuous love, patience, and support all through my education.

ABSTRACT

DEVELOPMENT OF REAL TIME BLOOD VESSEL IMAGING SYSTEM FOR EARLY DIAGNOSIS OF VASCULAR DISEASES

Disorders in the circulatory system may cause various diseases and tissue damage. The early detection of abnormalities in blood circulation has an important role in terms of treatment and also raising awareness of the patient. Vascular imaging methods used by today's technology are invasive, and/ or radiation-based. As an alternative to high-cost near infrared (NIR) vascular imaging devices in the market [1], a microcomputer-based, real-time, non-contact and safe vascular imaging system has been developed with low-cost.

Due to the higher absorption coefficient of blood than skin and fat and also the differences in the spectra of oxy and deoxyhemoglobin in blood, the vascular structures were obtained using light at NIR region. A device, which uses NIR LED light operated at 850 nm, was designed using optical and electronic components. Image and video analysis were performed using OpenCV, which is an open-source software library, and data visualization libraries. Tests were carried out to optimize the best imaging conditions for the device. To be able to show abnormalities in the vascular structures and to test the effectiveness of the device, "diabetes", which can cause various vascular disease complications, was selected. Superficial vascular structures were observed in the near infrared images captured from people at different stages of this disease.

As expected, the vessel images captured from the participants revealed deterioration in vascular structures in diabetic patients compared to healthy people. In order to make a clear inference about the accuracy of the images, it is necessary to compare them to the angiography images of the individuals and be interpreted by vascular surgery specialist.

ÖZET

DAMAR HASTALIKLARININ ERKEN TEŞHİSİ İÇİN GERÇEK ZAMANLI GÖRÜNTÜLEME SİSTEMİ GELİŞTİRİLMESİ

Dolaşım sistemindeki bozukluklar çeşitli hastalıklara ve doku hasarına neden olabilir. Kan dolaşımındaki anormalliklerin erken tespiti hem tedavi açısından hem de hastanın bilinçlendirilmesi açısından önemli bir role sahiptir. Günümüz teknolojisinin kullandığı vasküler görüntüleme yöntemleri, invazif ve / veya radyasyon tabanlıdır. Piyasadaki yüksek maliyetli yakın kızılötesi (NIR) vasküler görüntüleme cihazlarına bir alternatif olarak [1], düşük maliyetli, mikrobilgisayar tabanlı, gerçek zamanlı, temassız ve güvenli bir vasküler görüntüleme sistemi geliştirilmiştir.

Kanın deri ve yağa göre daha yüksek emilim katsayısı ve ayrıca kandaki oksijen ve deoksihemoglobin spektrumlarındaki farklılıklar sayesinde NIR bölgesinde ışık kullanılarak vasküler yapılar gözlemlendi. 850 nm'de çalışan NIR LED ışığı kullanan, bir cihaz, optik ve elektronik bileşenler kullanılarak tasarlandı. Görüntü ve video analizi, açık kaynaklı bir yazılım kitaplığı olan OpenCV ve veri görselleştirme kitaplıkları kullanılarak gerçekleştirildi. Cihaz için en iyi görüntüleme koşullarını optimize etmek için testler yapıldı. Damar yapısındaki anormallikleri gösterebilmek ve cihazın etkinliğini test etmek için çeşitli vasküler hastalık komplikasyonlarına neden olabilen "diyabet" seçilmiştir. Bu hastalığın farklı aşamalarındaki kişilerden alınan yakın kızılötesi görüntülerdeki yüzeysel vasküler yapılar gözlenmiştir.

Beklenildiği gibi, katılımcılardan alınan damar görüntüleri, diyabet hastalarında sağlıklı insanlara kıyasla damar yapılarında bozulmalar olduğunu ortaya koymuştur. Görüntülerin doğruluğu konusunda net bir çıkarım yapabilmek için kişilerin anjiyografi görüntüleriyle karşılaştırılması ve damar cerrahisi uzmanı tarafından yorumlanması gerekmektedir.

TABLE OF CONTENTS

LIST OF FIGURES	viii
LIST OF TABLES	x
LIST OF ABBREVIATIONS	xi
CHAPTER 1. INTRODUCTION	1
1.1. Medical Imaging Techniques.....	1
1.2. Vascular Diseases	2
1.3. Near Infrared Image Acquisition	4
1.3.1. Infrared Illumination	5
1.3.2. NIR Imaging Mode	6
1.4. Other Studies using Near Infrared Technology	9
CHAPTER 2. MATERIALS AND METHODS	10
2.1. Hardware Implementation	10
2.1.1. NIR Imaging Module.....	11
2.1.1.1. NIR Light.....	12
2.1.1.2. NIR Camera	12
2.1.1.3. Infrared Filter	13
2.1.1.4. Diffuser	14
2.1.1.5. Microcomputer.....	15
2.1.2. Device Design for 3D Modeling.....	16
2.2. Software Implementation.....	19
2.2.1. Grayscale Conversion	19
2.2.2. Contrast Limited Adaptive Histogram Equalization	20
2.2.3. Median Filtering	23
2.2.4. Frangi Filtering	23
CHAPTER 3. RESULTS AND DISCUSSION.....	26
3.1. Adjusting Lighting	26
3.1.1. Effect of Diffusers	26

3.1.2. Setting of Light Intensity	27
3.1.3. Effect of Daylight and Night Shoot on Image Acquisition Quality	31
3.2. Adjusting the Backdrop	32
3.2.1. Position of the LEDs.....	33
3.2.2. Position of the Target.....	33
3.2.3. Imaging Vascular Structures in Different Parts of the Body	34
3.3. Real-time Video Processing.....	35
3.4. Image Processing	37
3.5. Analysis of Images Captured from Volunteers.....	39
CHAPTER 4. CONCLUSIONS	48
REFERENCES	49

LIST OF FIGURES

<u>Figure</u>	<u>Page</u>
Figure 1.1. Absorption spectrum of oxy and deoxyhemoglobin	5
Figure 1.2. Reflection of light.....	6
Figure 1.3. Transmission of light.....	7
Figure 1.4. Side lighting	7
Figure 2.1. Block diagram of the hardware system.....	10
Figure 2.2. Operating structure of the system.....	11
Figure 2.3. Near infrared light	12
Figure 2.4. Parts of near infrared light.....	12
Figure 2.5. Near infrared camera module	13
Figure 2.6. Infrared filter used to transmit light in the near infrared wavelength range before capturing the image using camera.	13
Figure 2.7. HOYA infrared filter light transmission graph	14
Figure 2.8. Diffusers used to diffuse NIR light	14
Figure 2.9. Jetson nano module is the small microcomputer that we carry out the real-time data processing by connecting a display, keyboard and mouse.....	15
Figure 2.10. All parts of the device for 3D modeling.....	16
Figure 2.11. The output of all parts of the device.....	17
Figure 2.12. 3D Model of the device	17
Figure 2.13. Print out of device	18
Figure 2.14 Print out of device with diffusers	18
Figure 2.15. Structure of regions divided into 64 identical frames	21
Figure 2.16. The neighborhood structure of inner regions	22
Figure 2.17. The neighborhood structure of a corner region	23
Figure 3.1. Daylight images with 2 NIR LEDs, LEDs and camera are aligned at the same axes.....	27
Figure 3.2. Images captured by changing the quantity of NIR LEDs while the camera and target are fixed	28
Figure 3.3. The process on the images captured using 1 and 2 NIR LEDs	28
Figure 3.4. Schematic of the NIR LED	29
Figure 3.5. Resulting of different positions of trim potentiostat on 2 NIR LEDs	30

Figure 3.6. LEDs and camera are aligned at the same axes, night and daylight images captured with 2 NIR LEDs	32
Figure 3.7. Images captured by changing the angle of the 2 NIR LEDs using a black backdrop.....	33
Figure 3.8. Images captured by changing the distance of the target to the camera	34
Figure 3.9. Hand and arm images captured after making adjustments to the device	35
Figure 3.10. Block diagram of the real-time video processing.....	36
Figure 3.11. Monitor screen showing the infrared image of a foot. The device is located next to the monitor.....	36
Figure 3.12. A screenshot of the real-time foot image captured and processed on the monitor.....	37
Figure 3.13. Results of Frangi Hessian based vessel enhancement filter used to extract coronary arteries from coronary artery images obtained by X-ray angiography.....	38
Figure 3.14. Block diagram of the image processing	38
Figure 3.15. Image processing.....	39
Figure 3.16. Image processing applied to foot images of elderly diabetic person “Patient I” with toe amputation due to diabetic foot.	41
Figure 3.17. Vascular structure of the elderly diabetic person (Patient I)	42
Figure 3.18. Image processing applied to foot of a middle-aged person (Patient II)	43
Figure 3.19. Vascular structure of a middle-aged person (Patient III)	44
Figure 3.20. Image processing applied to foot of a healthy young person (Healthy I) ..	45
Figure 3.21. The vascular structure of a healthy young person (Healthy I)	46
Figure 3.22. The vascular structure in a young person (Healthy II).....	47

LIST OF TABLES

<u>Table</u>	<u>Page</u>
Table 1.1. Biometric identifications systems.....	8
Table 2.1. Jetson Nano Specifications	15



LIST OF ABBREVIATIONS

CT	Computed Tomography
MRI	Magnetic Resonance Imaging
MRA	Magnetic Resonance Angiography
CTA	Computed Tomography Angiography
CHD	Coronary Heart Disease
PAD	Peripheral Artery Disease
RHD	Rheumatic Heart Disease
PE	Pulmonary Embolism
DVT	Deep Vein Thrombosis
HbO	Oxyhemoglobin
HbR	Deoxyhemoglobin
ID	Identity
LED	Light-Emitting Diode
NIR	Near Infrared
RGB	Red, Green, Blue
CLAHE	Contrast-Limited Adaptive Histogram Equalization
IR	Inner Region
BR	Border Region
CR	Corner Region
DSA	Digital Subtraction Angiography
LDR	Light Dependent Resistor
HSV	Hue, Saturation, Value

CHAPTER 1

INTRODUCTION

This study focuses on near infrared technology for vascular imaging. In the first part of this section, conventional medical devices and the use of near infrared lighting with these instruments will be overviewed. After giving a brief definition of vascular diseases, their causes and symptoms, the studies utilize near infrared techniques for vascular diseases will be summarized. Finally, the details of the near infrared imaging technology will be discussed.

1.1. Medical Imaging Techniques

Vascular imaging plays an important role in clinical diagnosis and management of a variety of diseases and conditions. There are various vascular imaging techniques such as tomography, vascular ultrasound, magnetic resonance imaging and angiogram. Tomography is an imaging technique that takes images of the deep internal structures of the body from different angles in sections and then combines these sections to obtain 3-dimensional X-ray images. Tomography can give high resolution images of vascular structures but it's not practical for everyday use since ionizing radiation can be harmful for long term use and also need to use iodinated contrast to enhance the visibility of vascular structures [2]. Vascular ultrasound can be used for vascular imaging, but it costs high and needs additional trained staff [3]. Magnetic Resonance Imaging is a technique that is used to obtain images of soft tissues, the inner parts of the body in general, rather than imaging blood vessels. These non-radiation devices have high costs and also are not practical for portable uses since they require a dedicated space for the imaging and control equipments [4]. Angiogram is a 3D scanner for monitoring blood vessels that uses X-rays. Computed tomography angiography (CTA) needs a contrast agent to be administered through the vascular access in order to visualize the vascular structures [5].

In the magnetic resonance angiography (MRA) technique, contrast agent is not required, but it might be used for high resolution imaging [6]. Near infrared (NIR) method is another technique for vascular imaging. Target area is illuminated by NIR light where it penetrates through the skin and absorbed by hemoglobin present in blood vessels more than other surrounding tissue. At 850 nm, the absorption peaks have maximum for both oxy and deoxyhemoglobin. In addition, their difference with skin and fat tissues are higher than at other wavelenghts in the NIR region. Therefore, vessels appear darker [7,8]. It can be said that it is more advantageous to visualize vessels at 850 nm. There are many studies of NIR vascular imaging mainly for identity matching [9–11] and authentication based applications [12,13]. Unlike many studies focusing on using NIR imaging technology for security applications (finger and palm vein detection), our primary goal here is to utilize this technology for medical diagnosis purposes. Even though there are some methods used NIR imaging beyond security and investigate vascular structures for medical diagnosis [14,15] it is still highly desirable to design non-contact and a low-cost NIR imaging based medical device with real-time image analysis capability.

1.2. Vascular Diseases

Vascular diseases can cause serious disability and death as a result of abnormal condition in the blood vessels, which provide blood circulation in the body. There are many types of vascular diseases as listed below:

- “Coronary Heart Disease” (CHD) is caused when the blood vessels, which supply blood and oxygen to the heart, are narrowed.
- “Cerebrovascular Disease”, which is a disorder of the blood vessels that supply the brain. “Peripheral Artery Disease” (PAD) is caused by the inability to provide sufficient blood flow to the limbs, especially the legs, as a result of the narrowing of the blood vessels that feed the arms and legs.
- “Rheumatic Heart Disease” (RHD) that causes damage to the heart muscle and valves due to rheumatic fever.
- “Congenital Heart Defect”, which is a defect in the heart or blood vessels at birth.

- "Pulmonary Embolism" (PE) is a disease that occurs when blood clots called "Deep Vein Thrombosis" (DVT), which are found in blood vessels and have the potential to break free, travel to the lungs (WHO, 2017).
- "Superficial Venous Thrombosis" is inflammation and clotting in the vessels near the skin surface.
- "Chronic Venous Insufficiency" is a disease in which blood is pooled at the lower side due to the effect of gravity of the veins or a blockage in the leg as a result of damage to the unidirectional valves in the leg veins.
- "Varicose", is a disease that occurs with the enlargement of the vein in the superficial and deeper layers.
- "Ulcers" cause non-healing wounds or open wounds as a result of chronic venous insufficiency.

In addition to many causes of vascular diseases such as smoking, obesity, advanced age, unhealthy diet, insufficiency of physical activity, diseases such as "Diabetes", "Hypertension" and "High Cholesterol" are among the causes of vascular diseases. As in many diseases, early diagnosis is very important in vascular diseases. In this study, our aim is to develop a system where people who are at risk can follow their vascular health regularly, safely and easily. In this study, diabetes causing various vascular complications were investigated.

Diabetes mellitus is one of the most common chronic diseases globally. In 2019, an estimated 463 million adults had diabetes [16]. Glucose, which is the main fuel of our body, is broken down in the intestine by food and passes into the blood. High sugar in the blood is transferred to the cells by the hormone of insulin secreted by the pancreas. Increased sugar in the blood due to insulin deficiency or malfunction in the body is called diabetes mellitus. The increased amount of sugar in the blood begins to damage organs.

Diabetes can cause various complications. One of them is "Peripheral artery disease", which causes clogging of the vessels and reduced blood flow. Another type is the nerve damage known as "peripheral neuropathy". The third type is "diabetic foot ulcer", which is the most common cause of foot amputation in the world. Decreased blood flow as a result of complications can slow the healing of wounds. If the infection cannot be stopped, tissue damage or gangrene may occur and any existing infection can spread to the bone. In this case, amputation will be required. The most common amputations in

people with diabetes are toes, feet, and lower limbs. Diabetic foot infections are costly complications such as frequent hospital visits, daily wound care and treatment [17].

Vascular evaluation is important to detect patients with high risk of amputation. Detection of reduced or impaired blood circulation in the diabetic foot is necessary to prevent and cure an amputation that may occur [18–21].

1.3. Near Infrared Image Acquisition

The near-infrared (NIR) light wavelength range is approximately between 700-900 nm and is not seen by human eyes [22]. They are commonly generated by lasers and LEDs (light-emitting diodes). NIR light is non-ionizing, because it is in the part of the electromagnetic spectrum where there is not enough energy to cause ionization. This reduces the possibility of tissue damage. It also has the potential to light protection, photobiomodulation therapy of patients with depression, and turn into a safe and effective treatment for various diseases for instance Alzheimer's and Parkinson's. Therefore, NIR devices are a positive alternative for human applications [23–26].

In near infrared imaging, infrared light is sent from the device to the region of interest selected in the body. When light is sent suitable angle and distribution, it is captured and absorbed by the hemoglobin in the blood vessels. The higher absorption coefficient in the blood than skin and fat makes the vessels appear darker than the other tissues [27]. These dark vessels are captured by the infrared camera, processed in real time, and the vessels are made visible.

In the 600-1000 nm range, only in deoxyhemoglobin absorption, the peak value is observed in a place close to 750nm [22]. However, at 850nm, the blood vessels the more darker appearance than the surrounding tissue [28]. It provides a clear view of the vessel at this wavelength. that the wavelength at which the maximum density ratio between vascular and peripheral tissues is observed is better than the other wavelength. It is obvious that the wavelength (850nm) at which the maximum intensity ratio between the vascular and peripheral tissues was observed is better than the wavelength at which high absorption of hemoglobin occurs for vascular imaging.

1.3.1. Infrared Illumination

The main absorbers of NIR light in the blood are oxyhemoglobin (HbO) which is the oxygen-loaded form of hemoglobin and deoxyhemoglobin (HbR) which is the form of hemoglobin without oxygen. The absorption spectra of oxy and deoxyhemoglobin for between 600 and 1000nm has been shown in Figure 1.1. HbO absorbs more IR light and transmits more red light than HbR. HbR transmits more IR light and absorbs more red light than HbO. This allows us to see changes in light absorption at different wavelengths for the two types of hemoglobin [34]. The region "Near Infrared Region" is located in the electromagnetic spectrum, from about 700 to 900nm, where light absorption is minimal (Figure 1.1). After all, light in this wavelength range allows noninvasive investigations to be performed.

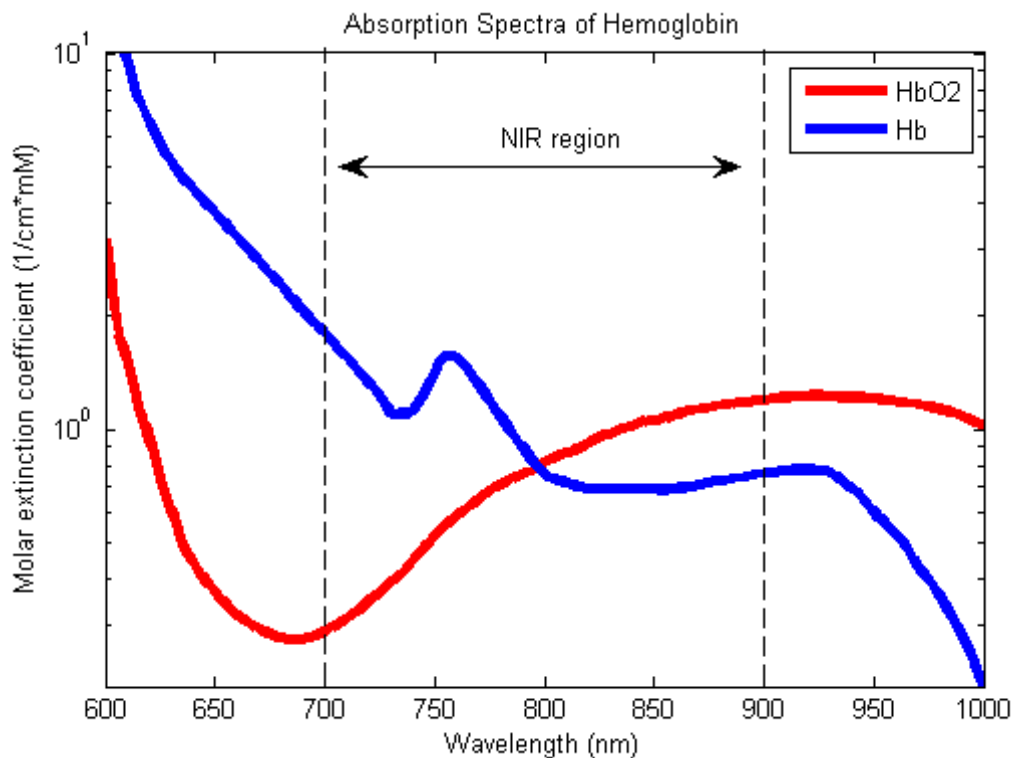


Figure 1.1. Absorption spectrum of oxy and deoxyhemoglobin [22].

1.3.2. NIR Imaging Mode

In the previous studies, different methods have been used as the vessels capture system. The first two of these are the typical methods, “reflection of light” (Figure 1.2) and “transmission of light” (Figure 1.3), and the third method is the “side lighting” (Figure 1.4) proposed by Hashimoto et al. [35].

In the light reflection application, there is no object between the device used and the region where the vascular image is captured. Here, the infrared light absorbed by the blood vessels makes the vascular structures appear dark. The image is captured by an optical device such as an infrared camera.

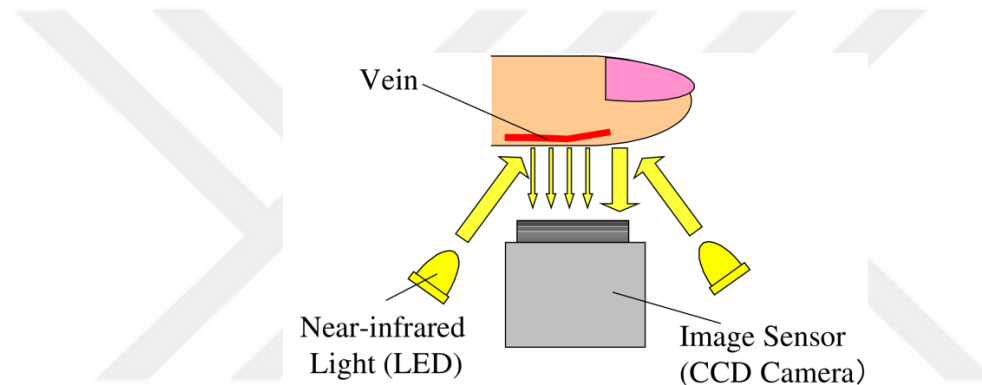


Figure 1.2. Reflection of light [35].

The reflection method is the most suitable method to image in large parts of the human body and also to be able to design a device with a small footprint. For this reason, the preferred method in our study was a reflection.

Light transmission application is an effective method to obtain a high contrast image in vascular imaging. Here, the light passes through the skin directly without spreading and the light energy is not lost, it can be said that the light is transmitted approximately 100%. The application may not be suitable for vascular imaging in areas other than body regions with appropriate thickness and volume. The size of the device proposed for this method may be a large device due to the location of the sensor and the light source.

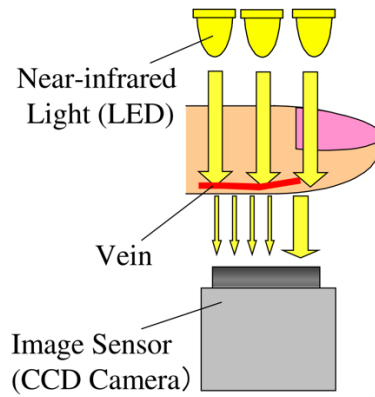


Figure 1.3. Transmission of light [35].

In the side lighting method, light is placed on both sides of the region to be displayed and the angle between the infrared camera and the infrared light is set to be ninety degrees. The light that enters the region to be illuminated from two sides is scattered in the blood vessels under the skin and then captured by the camera as after transmission.

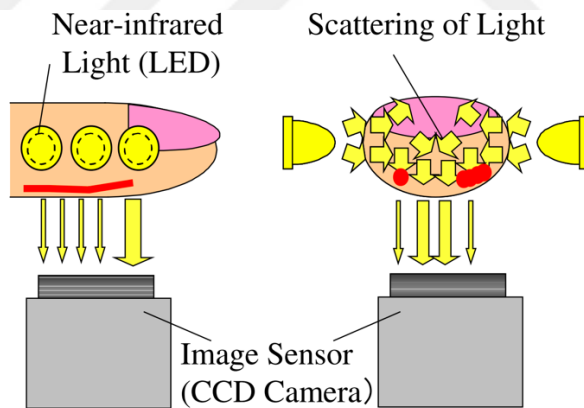
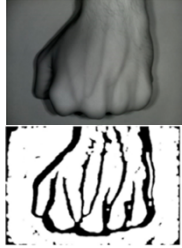
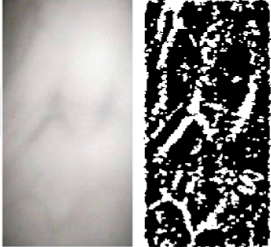
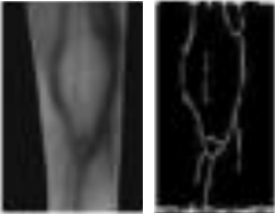

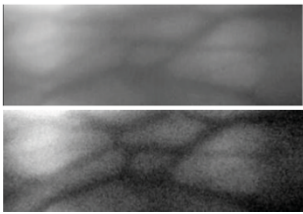


Figure 1.4. Side lighting [35].

Table 1.1. Biometric identifications systems.

Reference	Year	Processing	Raw and Result Images
Development of a low-cost microcomputer based vein imaging system [36].	2019	<ul style="list-style-type: none"> - Grayscale conversion - CLAHE - Median filtering - Adaptive thresholding - Binarization 	
Real Time Injecting Device With Automated Robust Vein Detection Using Near Infrared Camera And Live Video [37].	2017	<ul style="list-style-type: none"> - Grayscale conversion - Salt-pepper noise removing - CLAHE - Contrast adjustment - Adaptive thresholding 	
Cryptosystem Based On Finger Vein Patterns Using Vas Algorithm [38].	2016	<ul style="list-style-type: none"> - ROI extraction - Grayscale conversion - Gaussian filtering - Otsu's segmentation - Guided filtering - Gabor filtering - Global thresholding - Morphological func. - Thinning 	
Hand Vein Detection using Infrared Light for Web based Account [39].	2015	<ul style="list-style-type: none"> - Normalization - Binarization - Median filtering - Segmentation - Pattern thinning 	
Finger Vein Recognition Using Linear Kernel Entropy Component Analysis [40].	2012	<ul style="list-style-type: none"> - ROI extraction - CLAHE - Normalization 	

1.4. Other Studies using Near Infrared Technology

NIR light based vascular imaging has been used in many studies, mainly for security application such as ID matching and authentication. Hand and finger vein structures are unique for every individual, and cannot be changed or replicated [36,37]. Furthermore, it is difficult to hide or damage the structures because they are located under the skin, and also, finger veins can only be caught from a living body, so it is impossible to steal an ID of a dead person. Hence, both vein images are used for security application.

Our aim in this study is to design a device that obtains images of the vascular structures using near infrared light at low-cost and to monitor these processed frames in real-time. Inspired by methods used for NIR-based biometric identification systems, such as contrast adjustments, filters, our method employs similar approaches to produce high quality images. Some of these methods and processed images are given in Table 1.1.

It has been reported in current studies that near infrared light penetrates to depths of the skin between 2.6 and 15 mm [14], [28– 32]. The depth of the hand and foot superficial vessels ranges from 2 to 4.1 mm [33]. Therefore, we think that the images taken with our device can image the depth approximately 2.8 - 4 mm under the skin. We believe the observed depth can be increased with different methods, such as light transmission, where the light pass through the human body.

CHAPTER 2

MATERIALS AND METHODS

Our work consists of two parts as hardware and software. This part of the thesis includes the components we use for the hardware of our device, the mathematical description of the software used in the acquired images, the 3D modeling and output of our device.

2.1. Hardware Implementation

In this study, a black curtain is used as a backdrop for imaging. The distance between backdrop and camera is 60 cm. LEDs are in line with the camera. The target area where the vascular image to be captured should stand on the platform, and 15 cm away from the device. The block diagram of the system is shown in Figure 2.1. Also, the working structure of the hardware system is shown in Figure 2.2.

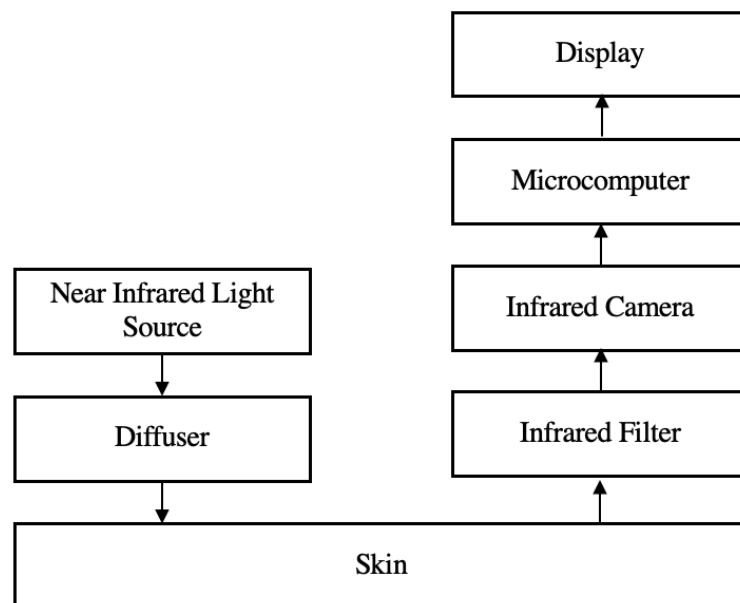


Figure 2.1. Block diagram of the hardware system.

The system has a simple operating principle. The infrared light emitted from the NIR light source is scattered by diffusers. Light is absorbed by the hemoglobin in the blood vessels in the target area, causing the blood vessels to appear darker. The infrared filter transmits the image to the camera. The image is acquired by the display connected to the camera and processed by the microcomputer.

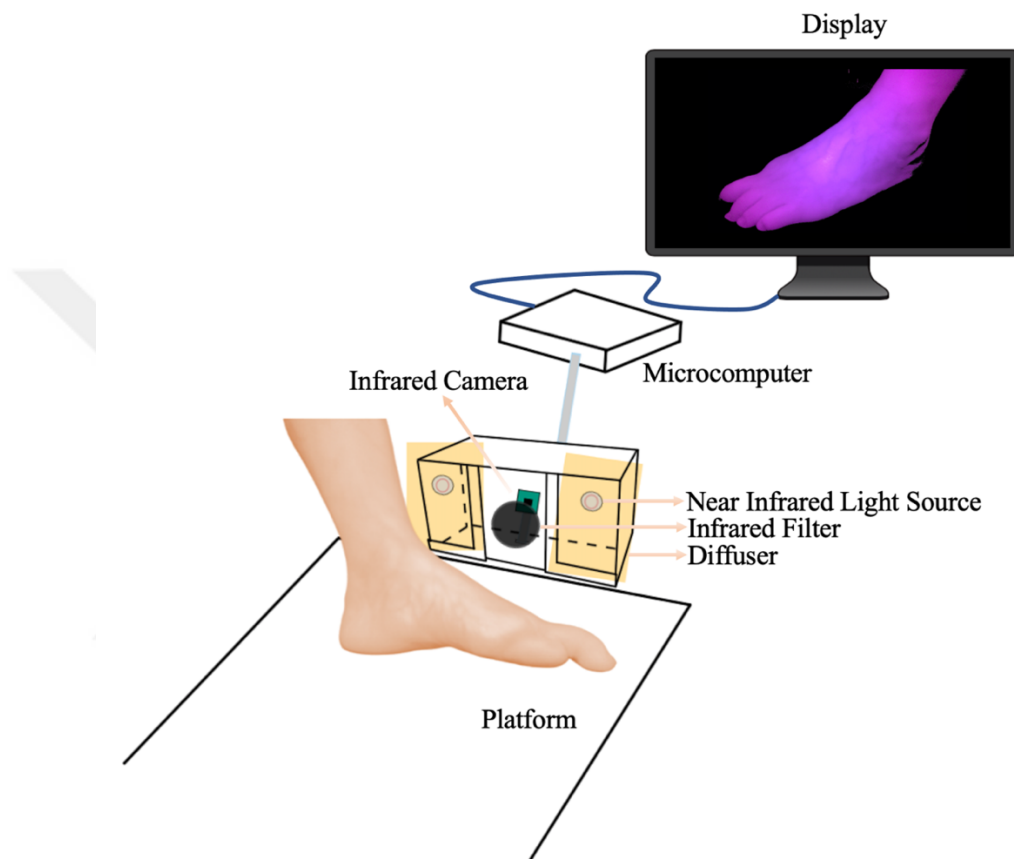


Figure 2.2. Operating structure of the system (sketched in [43]).

2.1.1. NIR Imaging Module

The designed system is low-cost and consists of parts that can be easily acquired. The hardware part of the system mainly covers two parts as lighting and image capturing. The materials used for these two parts are infrared light, infrared camera module, infrared filter, diffusers and microcomputer.

2.1.1.1. NIR Light

Infrared light is a 1W high power infrared illuminator module with 850 nm wavelength [44], adjustable resistance, light dependent resistance (LDR) and lens (Figure 2.3). The coverage allows the light to diffuse. Screw can be adjusted with a small screwdriver to change the brightness of the daylight and night light sensitivity threshold (Figure 2.4).



Figure 2.3. Near infrared light (850 nm).

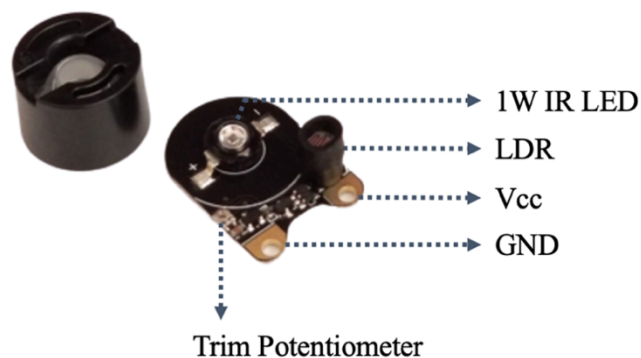


Figure 2.4. Parts of near infrared light.

2.1.1.2. NIR Camera

Raspberry Pi NoIR Camera Module (Figure 2.5) is an 8-megapixel Sony IMX219 image sensor, which has a fixed focus lens without an infrared filter. The camera is capable of 3280 x 2464 pixels static display and also supports 1080p30, 720p60 and 640x480p60 / 90 video [45]. Supported by Jetson Nano, this camera connects to the small

socket on top of the card via a ribbon cable and uses a special CSi interface specifically designed to interface with cameras. The size and small weight of the camera provides convenience for many applications.

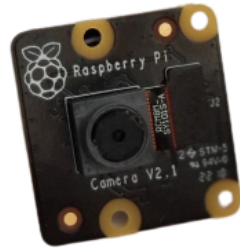


Figure 2.5. Near infrared camera module.

2.1.1.3. Infrared Filter

Infrared filters are special filters designed to pass light in the near infrared wavelength range of 700-900 nm on average. In our study, 49 mm 720 nm infrared filter (Hoya 49 mm R72) was used as shown in Figure 2.6.



Figure 2.6. Infrared filter used to transmit light in the near infrared wavelength range before capturing the image using camera.

HOYA infrared filter transmits 95% of the light in the range of 760 nm – 860 nm (Figure 2.7). Infrared filter was used to eliminate ambient light to be able to acquire images during daylight [39].

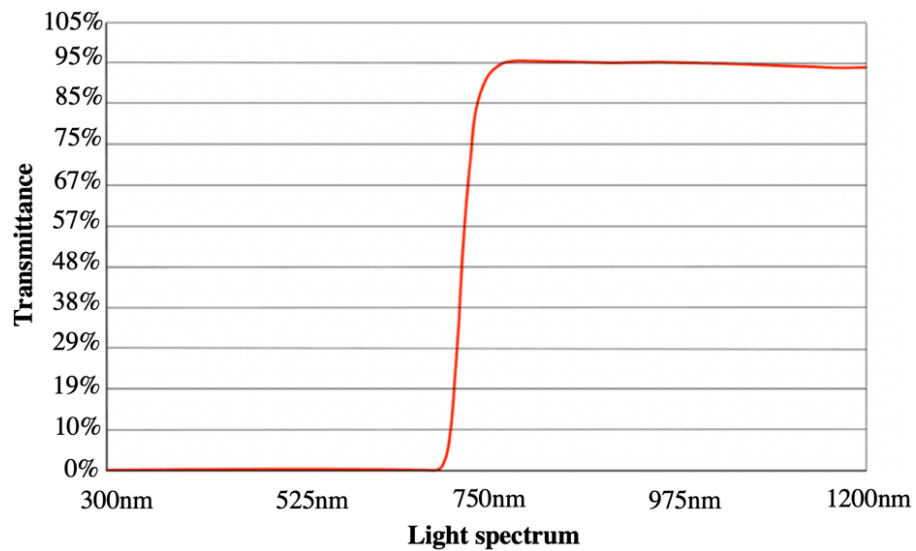


Figure 2.7. HOYA infrared filter light transmission graph [46].

2.1.1.4. Diffuser

Diffusers are optical components that are used to improve the smoothing of the illumination intensity, to diffuse the light and to provide a better visualization (Figure 2.8). In this study, "Yongnuo YN160 / YN300 Led Light Compatible Diffuser" was chosen [47].



Figure 2.8. Diffusers used to diffuse NIR light. The difference in colors effects the amount of diffused light. The orange diffuses the light more than white (orange was used in the study).

2.1.1.5. Microcomputer

The Jetson Nano module, 70 x 45 mm in size, is the smallest microcomputer among Jetson devices. Since Jetson Nano has low power consumption (5-10 watts) and high processing power up to 472 GFLOPS, it can quickly run image processing, machine learning algorithms. Table 2.1 can be examined for detailed specifications [48]. Jetson Nano consist of microSD card slot, 40-pin expansion header, micro-USB port, gigabit ethernet port, 4 USB ports, HDMI output port, display port connector, DC barrel jack for 5V power input and CSI camera connectors (Figure 2.9).

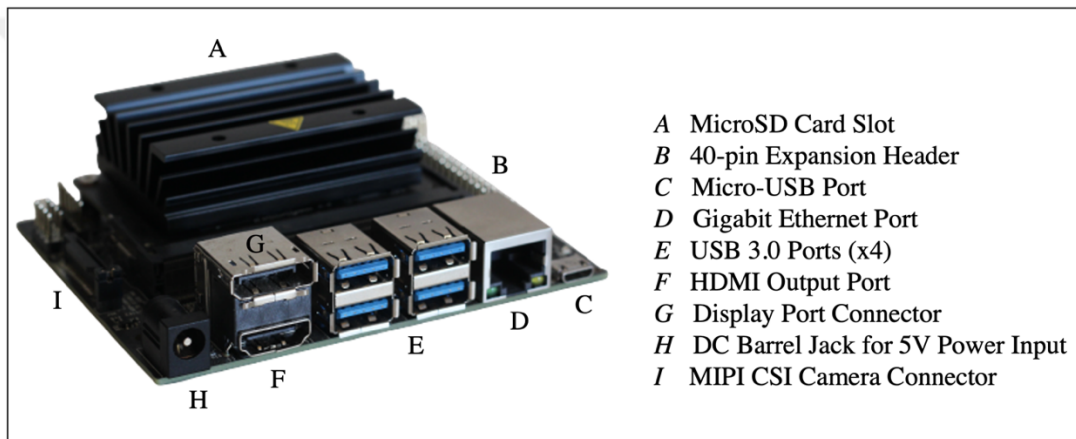


Figure 2.9. Jetson nano module is the small microcomputer that we carry out the real-time data processing by connecting a display, keyboard and mouse.

Table 2.1. Jetson Nano Specifications

GPU	128 Core Maxwell 472 GFLOPs (FP16)
CPU	Quad-core ARM A57 @ 1.43 GHz
Video Encode	4K @ 30 fps, 4x for 1080p @ 30 fps, 9x for 720p @ 30 fps (H.264/H.265)
Video Decode	4K @ 60 fps, 2x for 4K @ 30 fps, 8x for 1080p @ 30 fps, 18x for 720p @ 30 fps (H.264/H.265)
Camera	MIPI CSI-2 and PCIe Gen2 high-speed I/O

2.1.2. Device Design for 3D Modeling

3D modeling of our device was realized with Blender, a free and open-source 3D creation suite. The model consists of the power bank box, the camera box and their lids. There is a holder inside the camera box to fix the camera. There are gaps in the width of the ribbon cable in the bottom of the camera holder and the box to allow the camera to connect with the microcomputer outside the box. In addition, holes for a filter and LEDs in the lid of camera box act as a holder for these parts, and also there are two holders to fix the diffusers. LED lights are powered by the power bank, thus a box for the power bank has been designed behind the camera box. Holes are opened at the power bank's lid to provide power output from the power bank and to recharge the power bank. There is also a space for the ON / OFF button on the power bank box. You can see all the parts of the modeling in detail in Figure 2.10, print out in Figure 2.11. The final version of the box's model is shown in Figure 2.12.

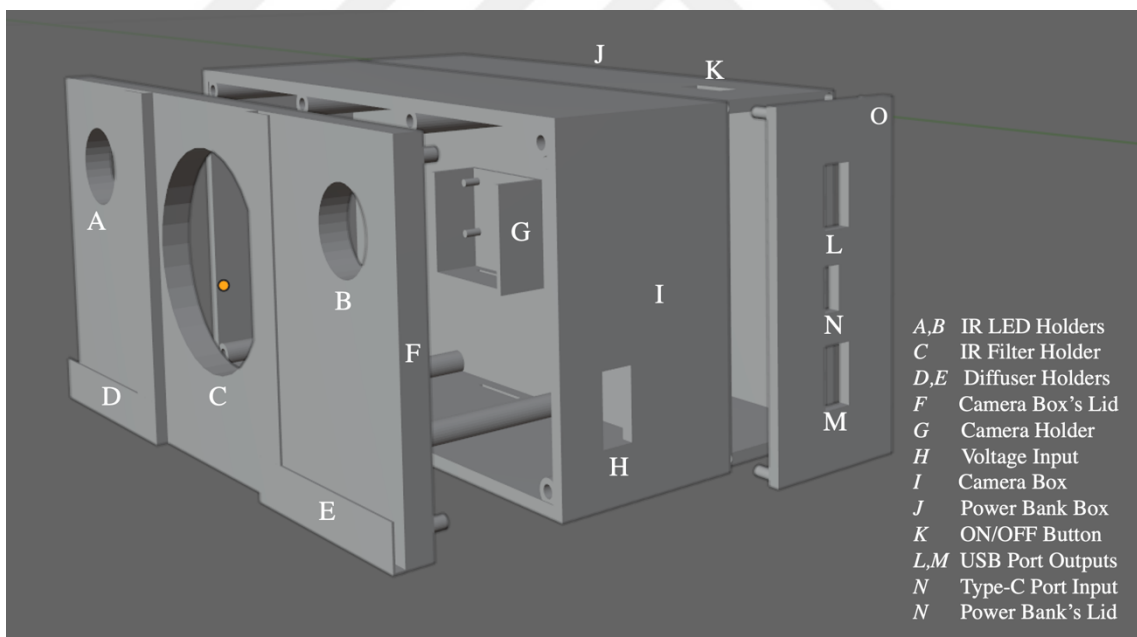


Figure 2.10. All parts of the device for 3D modeling. The lid part of the camera box holds the LEDs, infrared filters and diffusers. Inside the camera box there is a holder that holds the camera module and at the back of the camera box there is a box for the power bank that powers LEDs.



Figure 2.11. The output of all parts of the device. The lid of the camera box holds the LEDs, infrared filters and diffusers. There is a camera module in the holder inside the camera box, and there is a power bank box on the back of the camera box with the power bank that powers the LEDs.



Figure 2.12. 3D Model of the device.

The printout of our model was captured from a 3D printer and all components were placed. The LEDs were combined with the resistors inside the box, together with the USB cable coming from the power bank. Print out of device is shown in Figure 2.13, and the final model of device is shown in Figure 2.14.



Figure 2.13. Print out of device. LEDs powered by the USB cable coming from the power bank.

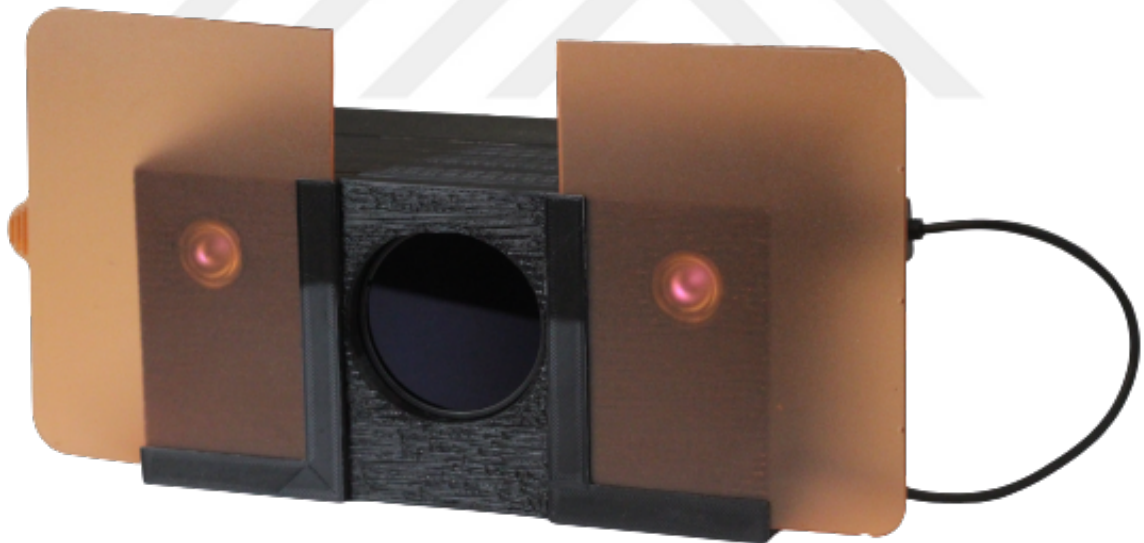


Figure 2.14 Print out of device with diffusers.

The cost of the system design, including microcomputer, NIR camera module, NIR LEDs, infrared filter, diffusers and power bank is approximately 2.400 Turkish liras (~300 U.S. dollars). When computer screen and all materials used for tests included, the cost did not exceed 5.000 Turkish liras (~600 U.S. dollars).

2.2. Software Implementation

In order to obtain clear vascular images, it is important to develop a robust image processing algorithm. Python programming language has been used to write the software program. Frames from real-time video were captured using microcomputer and were processed with OpenCV libraries. The process contains grayscale conversion, contrast-limited histogram equalization technique and median filter, a non-linear digital filtering technique. Separately, the Frangi filter was used to transform the vessels in the acquired images into tube-like structures.

2.2.1. Grayscale Conversion

Grayscale has smaller data than RGB images and is a useful option to shorten the processing time. When converting a colored image to a grayscale image, it is important that it does not lose its contrast, sharpness, shadow and structure. For this, an algorithm has been developed that preserves the properties of the image [49].

1. $Y = (0.299 \times R) + (0.587 \times G) + (0.114 \times B)$
2. $U = (B - Y) \times 0.565$
3. $V = (R - Y) \times 0.713$
4. $UV = U + V$
5. $R1 = R \times 0.299$
6. $R2 = R \times 0.587$
7. $R3 = R \times 0.114$
8. $G1 = G \times 0.299$
9. $G2 = G \times 0.587$
10. $G3 = G \times 0.114$
11. $B1 = B \times 0.299$
12. $B2 = B \times 0.587$
13. $B3 = B \times 0.114$
14. $R4 = \frac{R1 + R2 + R3}{3}$

15. $G4 = \frac{G1 + G2 + G3}{3}$
16. $B4 = \frac{B1 + B2 + B3}{3}$
17. $I1 = \frac{R4 + G4 + B4 + UV}{4}$
18. *END*

Here in the steps 1 to 3, Y, U, V components are calculated from R, G, B components and Y determines the luminance of the color and U and V determines the chrominance, which is the colorimetric difference between a standard color of equal brightness. Step 4 shows the sum of the chrominance value. Between steps 5 and 16, an approximate RGB (red, green, blue) value is calculated with the values obtained by using the RGB components and in step 17, I1 represents the gray color image obtained.

2.2.2. Contrast Limited Adaptive Histogram Equalization

Real-time image sequences may not have good quality due to factors such as distance, light intensity, and natural noise. In this case, it may be necessary to improve the image quality. Contrast limited adaptive histogram equalization is a technique used in medical imaging systems to increase regional contrast and has been proven to be useful [45,46]. In this approach, the image is examined by dividing it into regions of approximately equal size. To start with, the histogram of each region is calculated. In the second step, the clip limit is obtained according to the desired contrast window width for contrast expansion. In the third step, each histogram value is re-determined to prevent exceeding the specified clip limit. Finally, the cumulative distribution functions of the histograms are calculated for grayscale mapping. The image is divided into 8 equal parts horizontally and vertically and 64 parts are obtained. Regions are classified as three different group names; first group name is the corner regions (CR) in four corners, the border regions (BR), which consists of twenty-four border regions, and the remaining thirty-six inner parts, is called inner regions (IR) (Figure 2.15).

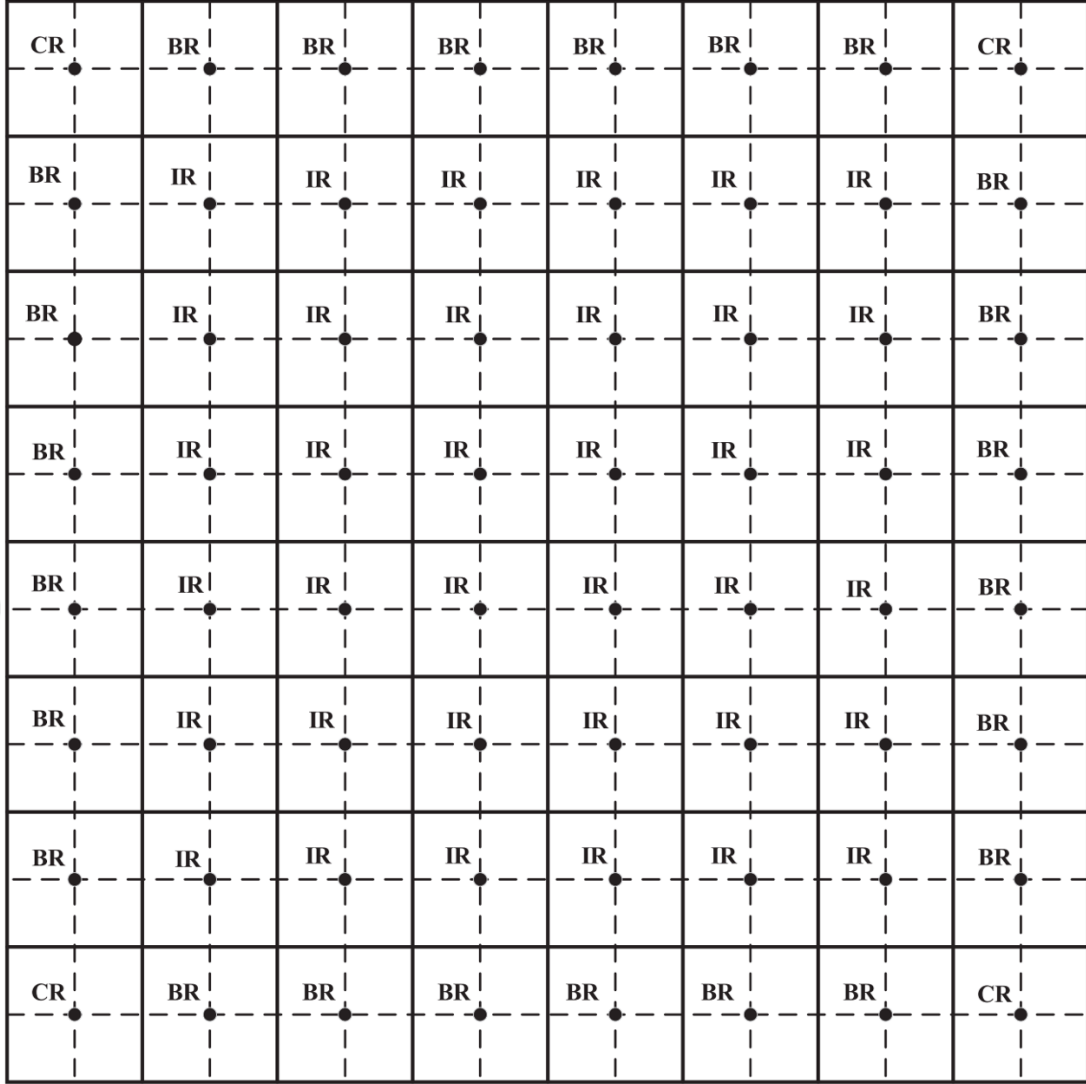


Figure 2.15. Structure of regions divided into 64 identical frames in a 512×512 image [52].

Each region is composing of four quadrants and have different number of neighboring. The number of neighbors of each part in the IR group is the same (Figure 2.16) and the new values of the pixels in this region are calculated by the equation given below:

$$\rho_{new} = \frac{s}{s+r} \times \left(\frac{y}{x+y} \times f_{i-1,j-1}(\rho_{old}) + \frac{x}{x+y} \times f_{i,j-1}(\rho_{old}) \right) + \frac{r}{r+s} \times \left(\frac{y}{x+y} \times f_{i-1,j}(\rho_{old}) + \frac{x}{x+y} \times f_{i,j}(\rho_{old}) \right)$$

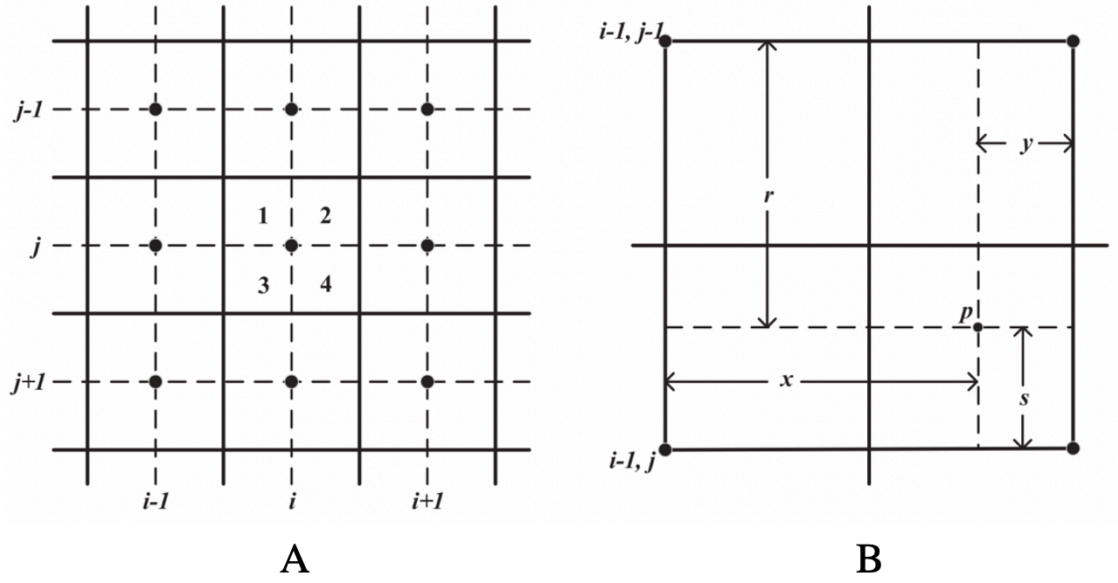


Figure 2.16. The neighborhood structure of inner regions **(A)** A given IR region with its all-neighboring regions. **(B)** The first quarter of (i,j) region and its relations with the closest four regions [52].

Considering the left part border regions in the BR group, the pixel calculation in the second and fourth quadrant is calculated in the same way as the pixel calculation in the IR. However, pixel values in the first and third quadrant are calculated by the following equation by their position:

$$\rho_{new} = \frac{s}{s+r} \times f_{i,j-1}(\rho_{old}) + \frac{r}{r+s} \times f_{i,j}(\rho_{old})$$

There are different features for quadrants in CR. Pixel values in the second and third quadrants are calculated by calculating the pixel value in the BR region. For the pixel values in the fourth quadrant, the pixel value calculation in the IR group is used. The top-left corner of the CR region and the quadrants with different features are shown in Figure 2.17. Since the first quadrant does not come into contact with other regions, the pixel values remain unchanged as given in the following equation:

$$\rho_{new} = f_{i,j}(\rho_{old})$$

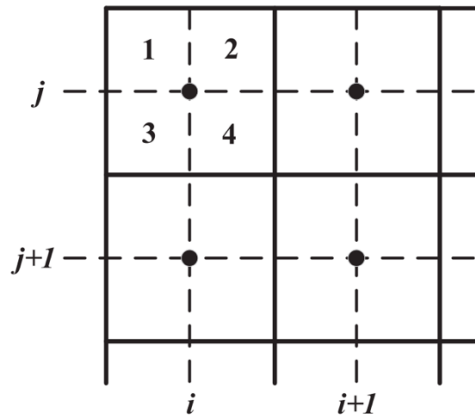


Figure 2.17. The neighborhood structure of a corner region [52].

2.2.3. Median Filtering

The images captured in real-time contain noises for different reasons. Median filter is a nonlinear filtering method that clears noise in images without interfering with edges and lines. In other processes to be performed after filtering, a more accurate vascular images will be obtained. In this method, each pixel is changed by the median of the pixels in neighboring regions. This operation is given by:

$$y [m, n] = \text{median} \{x[i, j], (i, j) \in \omega \}$$

ω represents the neighborhood of a pixel with location at $[m, n]$.

2.2.4. Frangi Filtering

Frangi filter is a filter that works based on the evaluation of the vascular structures in vascular images as a tube-like structure using eigenvalues analysis of Hessian matrix. These images are obtained by 2D projection techniques such as Digital subtraction angiography DSA and 3D methods such as X-ray rotational angiography, CTA, MRA.

By calculating the Gaussian second order derivative, the Hessian matrix in the point x at scale σ , $\mathcal{H}_\sigma(x)$, is calculated as follows:

$$\mathcal{H}_\sigma(I, x) = \frac{\partial^2 I_\sigma}{\partial x^2} = I(x) * \frac{\partial^2 \mathcal{G}_\sigma(x)}{\partial x^2}$$

I : the image

\mathcal{G}_σ : the gaussian function with the standard deviation σ .

The separation of the second-order structure of the image provides the extraction of eigenvalues ($|\lambda_1| \leq |\lambda_2| \leq |\lambda_3|$) and Hessian analysis has an intuitive reason for vascular detection.

A vesselness function, $\mathcal{V}_F^\sigma(x)$, was designed to measure the similarity of vascular structures of different sizes to an ideal tube by Frangi et al. [53]:

$$\mathcal{V}_F^\sigma(x) = \begin{cases} 0 & \text{if } \lambda_2 > 0 \text{ or } \lambda_3 > 0 \\ \left(1 - \exp\left(\frac{\mathcal{R}_A^2}{2\alpha^2}\right)\right) \exp\left(\frac{\mathcal{R}_B^2}{2\beta^2}\right) \left(1 - \exp\left(\frac{\mathcal{S}^2}{2c^2}\right)\right) & \text{else} \end{cases}$$

α, β, c : parameters that control the sensitivity of the filter and measures dissimilarity that distinguish between tube-like and plate-like structures (\mathcal{R}_A), blob-like (\mathcal{R}_B) and background (\mathcal{S}):

$$\mathcal{R}_A = \frac{|\lambda_2|}{|\lambda_3|}$$

$$\mathcal{R}_B = \frac{|\lambda_1|}{\sqrt{|\lambda_2 \lambda_3|}}$$

$$\mathcal{S} = \sqrt{\lambda_1^2 + \lambda_2^2 + \lambda_3^2}$$

According to the filter responses based on integrates at different scales, the vesselness is finally being estimated using the maximum response:

$$\mathcal{V}_F(x) = \max_{\sigma_{min} \leq \sigma \leq \sigma_{max}} \mathcal{V}_F^\sigma(x)$$

These methods were applied by microcomputer after the images were captured by the device. The results were summarized in the following chapter.



CHAPTER 3

RESULTS AND DISCUSSION

This section summarizes the test results of optical materials and the results of following adjustments such as intensity and angle of the light. Then, the appropriate position of the target was determined and the backdrop adjustment was made. After that, the vessel frames were captured and processed on real-time. Separately, Frangi filter used in angiography devices was applied to the images taken using the device. Finally, vessel images taken from volunteer participants were discussed.

3.1. Adjusting Lighting

Shadows and glare have an effect on the vessel images. Therefore, need to be minimized for good quality. For smooth adjustment of light, firstly, the effect of the diffuser was studied, and then the amount of LED lights was determined. Then, the effect of different light intensities on the image was tested. Finally, the images were collected at daylight and night and then compared.

3.1.1. Effect of Diffusers

Diffusers are used to distribute the light coming from the light source and soften the shadows. To be able to see the effect of the diffusers on infrared light illumination, in Figure 3.1(A), LEDs were reflected to the backdrop without diffusers. The raw image was converted to grayscale and then CLAHE was applied. The glare (indicated with a yellow arrow) that occurs after the process is clearly visible. Figure 3.1(B) shows that there is a noticeable reduction in glare when the image was captured by placing a diffuser in front of the LEDs without changing the position of the camera and LEDs and the same processes was applied.

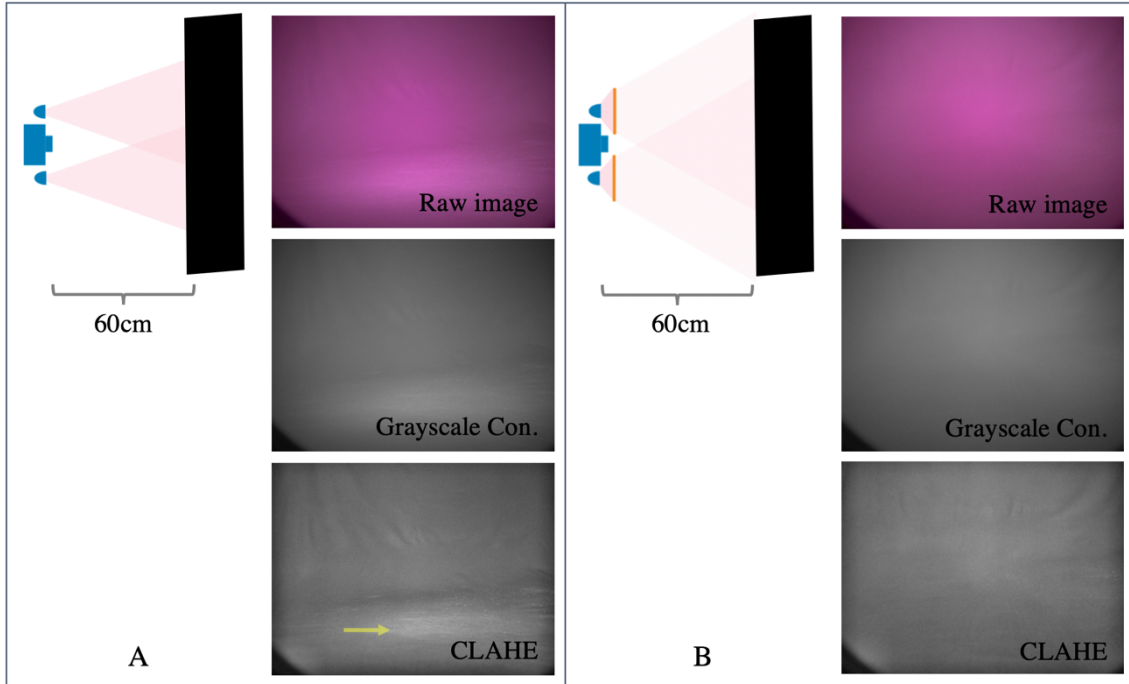


Figure 3.1. Daylight images with 2 NIR LEDs, LEDs and camera are aligned at the same axes (**A**) Images captured without diffuser. The glare (yellow arrow) that occurs after the process is clearly visible (**B**) Images captured with diffuser.

3.1.2. Setting of Light Intensity

Another factor in acquiring a good image is the amount of light reflected on the target. If the target is not illuminated sufficiently, there may be some data loss in the captured images. On the contrary, when it is illuminated too much, there might be glare and shadows, which will cause noise in the processed images.

In these tests where the camera and the target were kept constant, first of all, the number of LEDs used was changed and comparisons were made. Figure 3.2(A), (B), (C), and (D) raw images are captured with 1, 2, 3 and 4 LEDs respectively. The shadows are clearly seen in the images captured with 3 and 4 LEDs.

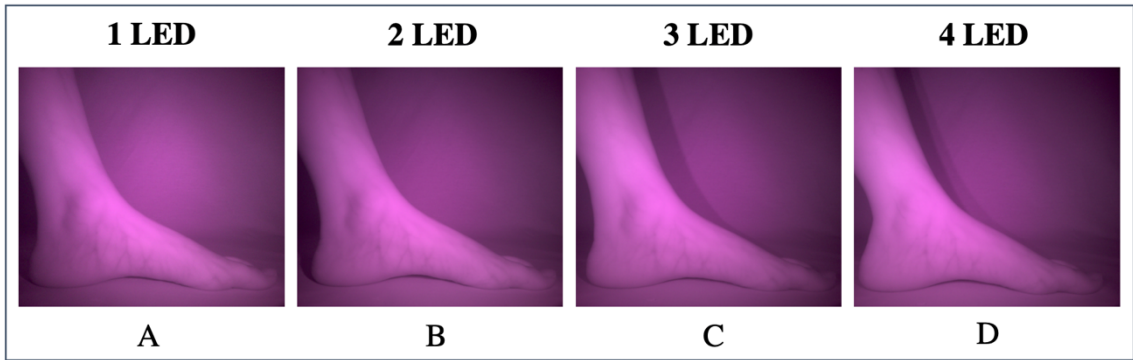


Figure 3.2. Images captured by changing the quantity of NIR LEDs while the camera and target are fixed (3,4 LEDs have shadow).

In order to see the effect of 1 and 2 LEDs in more detail, tests were carried out at different hours of 1 day and a similar result was reached. Figure 3.3 also clearly shows that the light intensity of 1 LED is not enough to illuminate the toe, ankle and heel of foot. According to this result, 2 LEDs were chosen for the study.

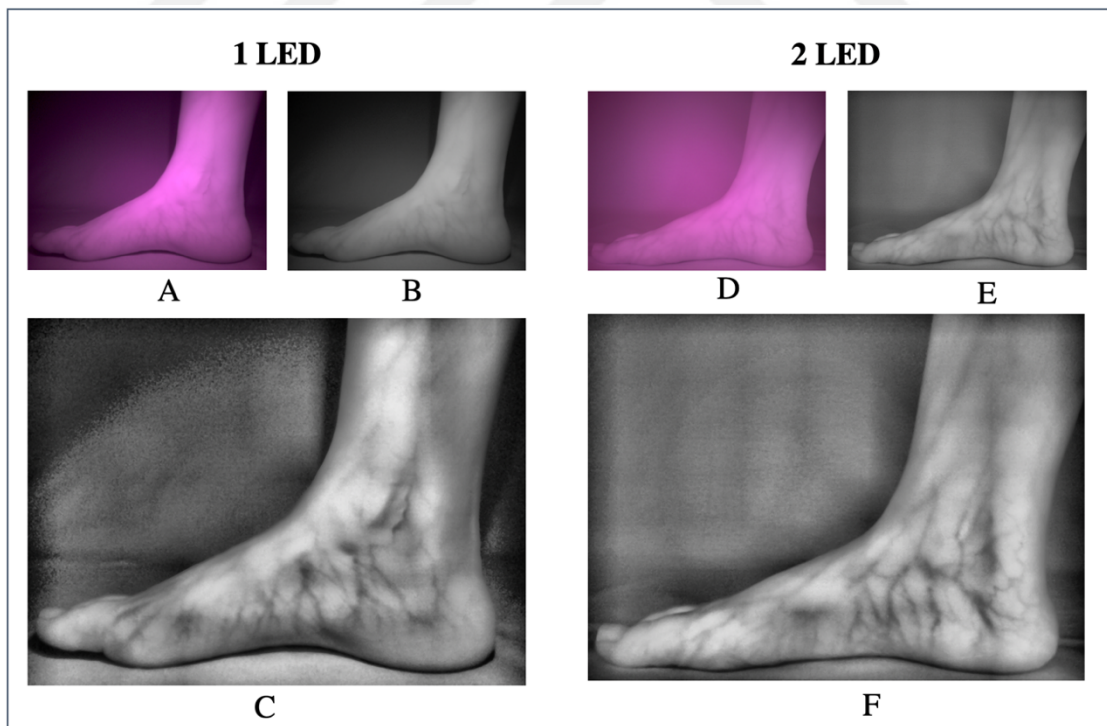


Figure 3.3. The process on the images captured using 1 and 2 NIR LEDs. (A,D) raw images, (B,E) grayscale conversion (C,F) CLAHE applied. The light is more diffuse in the images captured by 2 LEDs.

The schematic of the infrared LEDs used is given in Figure 3.4. The infrared LEDs are powered by the voltage from the power bank. There is a 2.5V regulator (MIC5219) in the circuit that is limited to 250mA and controls the overall output. The potentiostat used in the circuit adjusts the amount of ambient light to change the trigger point of the LED, that is, whether the LED is on or off. LDR is a photoresist and its resistance value change inverse proportion to the amount of light. Potentiostat change and the amount of ambient light falling on the LDR affect the base current to the transistor, which changes the light intensity of the infrared LED. Capacitor connected in parallel to the LDR used as a bypass AC signal to ground. For an AC signal, the capacitor is shorted and bypasses it. Thus, the capacitor reduces unwanted noise at the output. The capacitor passing DC behaves as if it is open to DC. The transistor pair in the circuit is the Sziklai Darlington pair, which consists of NPN and PNP complementary transistors in a configuration that provides power with lower impedance and also the current gain is equal.

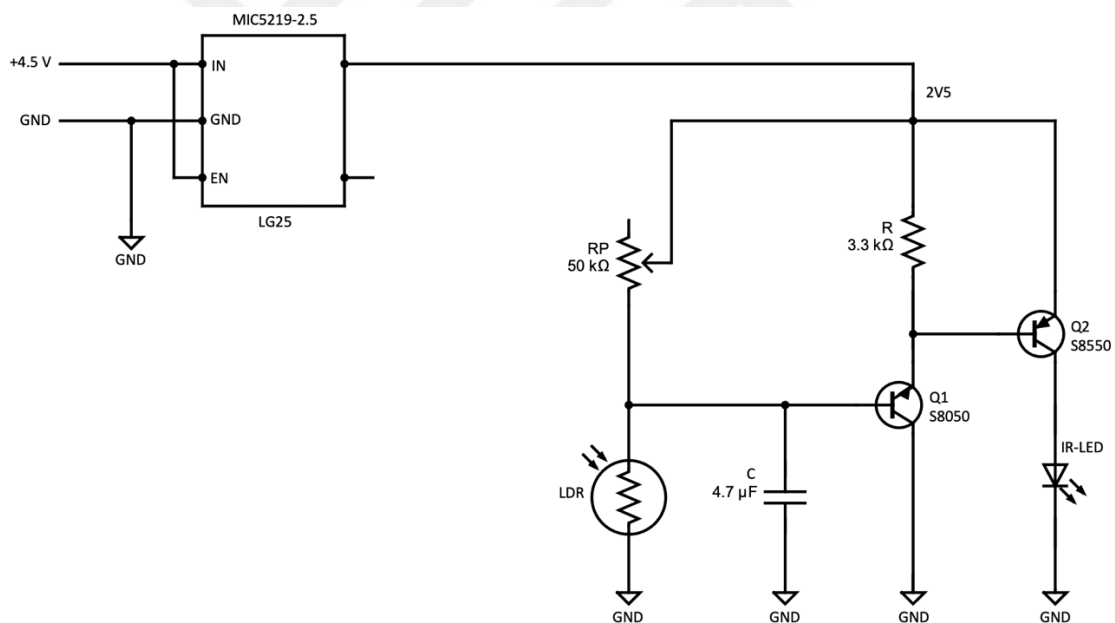


Figure 3.4. Schematic of the NIR LED (sketched in [54]).

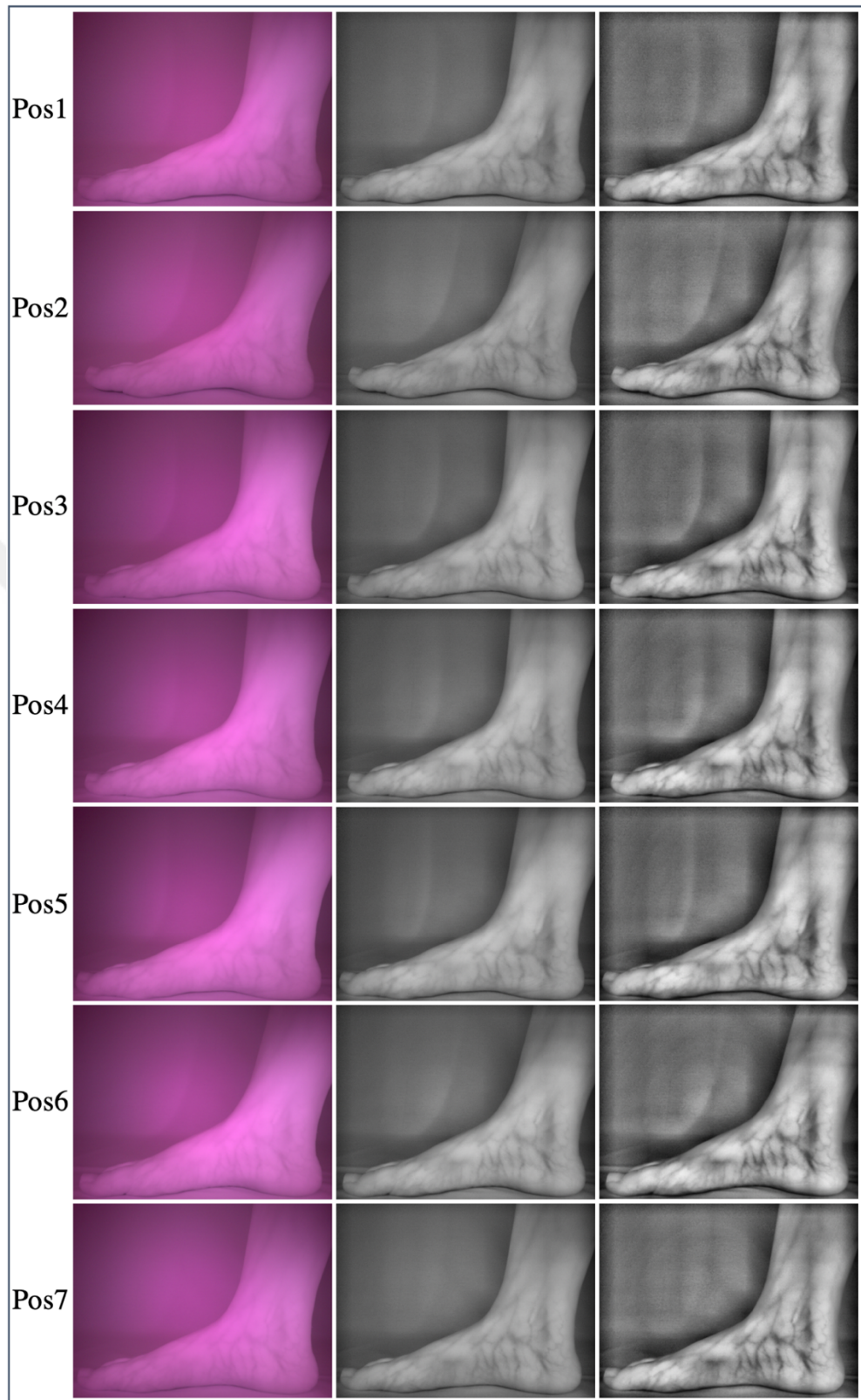


Figure 3.5. Resulting of different positions of trim potentiostat on 2 NIR LEDs. The light intensity increases from Pos1 to 7. Raw, grayscale conversion and CLAHE applied images for each position. The light is more diffuse in the images captured by Pos7.

In this study, we closed the LDR in the circuit with a black band, left it constant at the max resistance value and reduced the variable parameters. Thus, we were able to change the light intensity of the infrared LED by manually changing the potentiostat value, and we evaluated the images we took over this change (Figure 3.5). As the potentiostat value changes, the trigger current to the base of the NPN transistor (S8050) changes. Accordingly, the current flowing from the emitter of the NPN transistor to the collector changes, and this changes the current to the base of the PNP transistor (S8550). Thus, the current from the emitter of the PNP transistor to the collector also changes. As the current changes, the light intensity on the infrared LED (power of the infrared-LED) also changes. In short, the change of LED brightness is provided by an NPN controlled PNP transistor as a result of potentiostat change. The images captured and processed as Pos1 in Figure 3.5 are the potentiostat position where the light intensity of the LED is at minimum. The amount of light intensity towards Pos7 increases equally.

3.1.3. Effect of Daylight and Night Shoot on Image Acquisition Quality

The device we designed allows us to shoot in the sun with its infrared filter. In this section, night and daylight images were captured for comparison by keeping the camera target and LEDs fixed. The raw, grayscale conversion and CLAHE results of the captured images are given in Figure 3.6. When the two situations were compared, the distribution of light is much better in daylight images than at night. Even a small amount of data loss was observed in the images captured at night. As a result, daylight and night images can be captured with our device, but as a result of these tests, daylight images give better results.

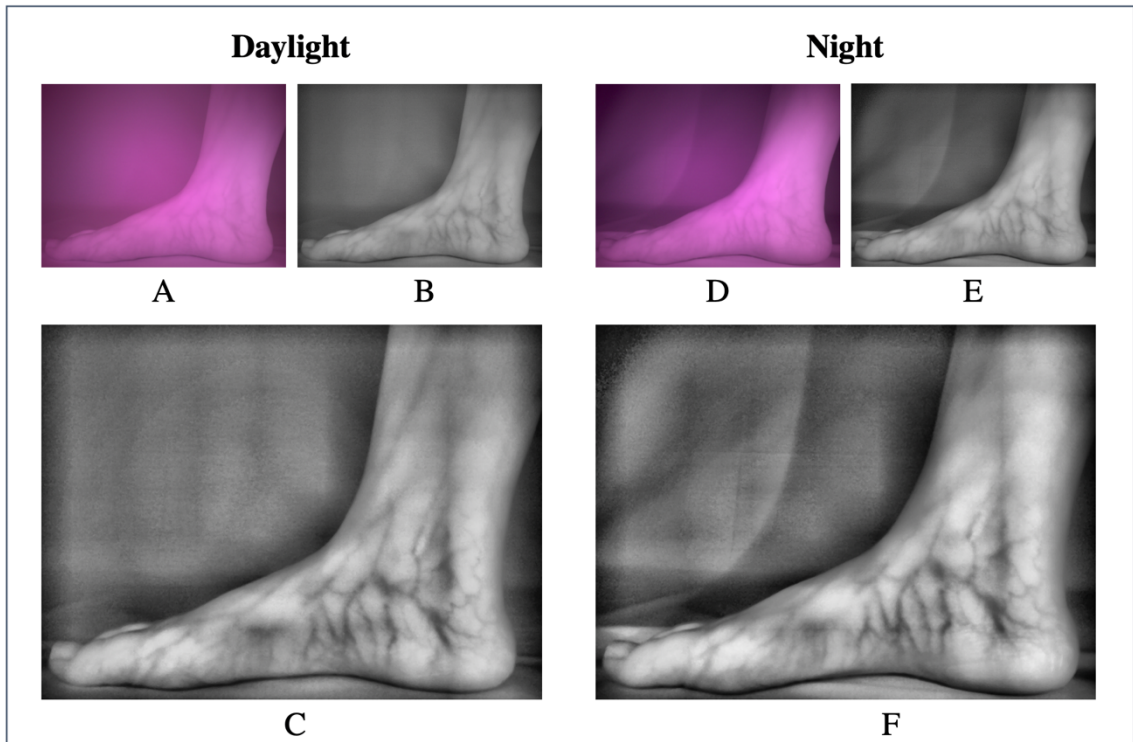


Figure 3.6. LEDs and camera are aligned at the same axes, night and daylight images captured with 2 NIR LEDs. *(A, D)* raw images, *(B, E)* grayscale conversion *(C, F)* CLAHE applied. Light is more diffuse in images captured in daylight.

3.2. Adjusting the Backdrop

In the previous part, tests were carried out on a white backdrop to make adjustments for smoothing the light illumination. In our study, a black backdrop is used in order not to reflect light and to extract the target easily. Both of the fabrics used for our backdrop are black in color, but due to the difference in the type of the fabric, the backdrop color varies in the appearance.

In this section, the used backdrop, the angle of the LEDs and the location of the target on the platform are determined. In addition, images of the hand and arm were captured with the final state of the system and the images captured were discussed.

3.2.1. Position of the LEDs

It is known that the angle of irradiated light affects the images captured [55]. Since we do not have the equipment to make a precise measurement here, the LED angle was adjusted in two different ways as an estimated 45 degrees and 90 degrees perpendicular to the target and evaluations were made on the images captured. It is clearly seen in the results in Figure 3.7 that the vascular structures in the images captured at 90 degrees is more pronounced than captured at 45 degrees.

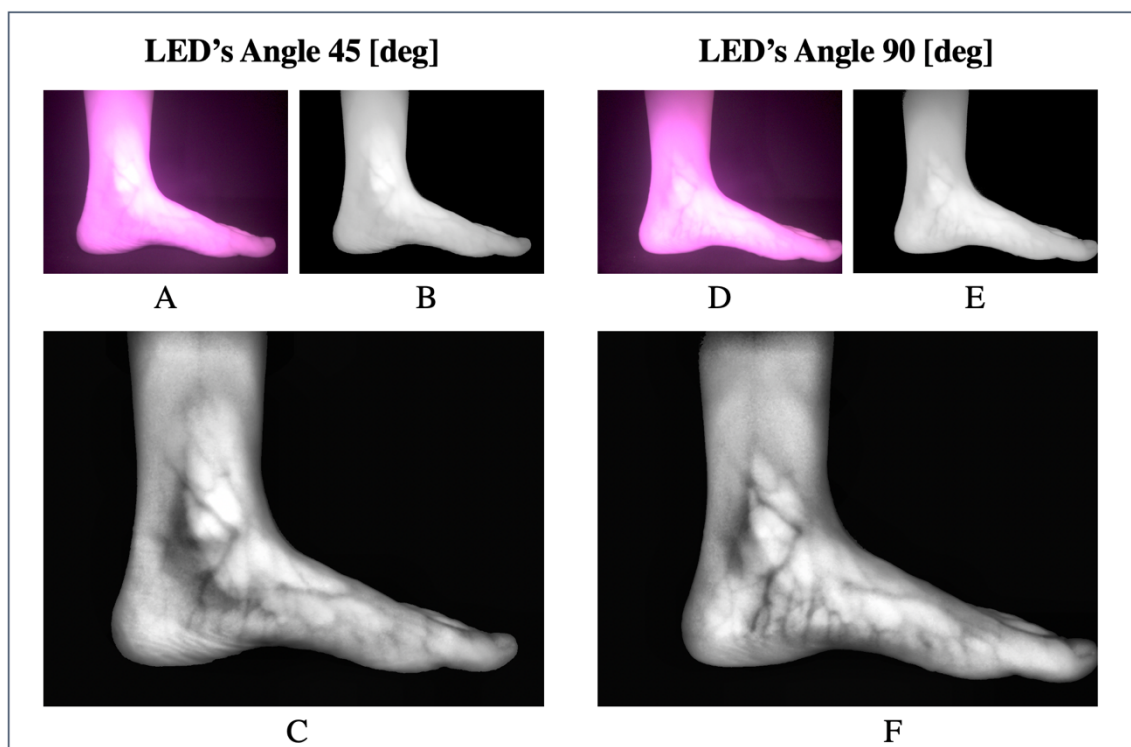


Figure 3.7. Images captured by changing the angle of the 2 NIR LEDs using a black backdrop. (A, D) raw images, (B, E) images with removed background, (C, F) CLAHE applied.

3.2.2. Position of the Target

Here it was discussed how the distance of the target from the camera affects the image. We observed glare and data loss increase as you move closer to the target backdrop

and away from the camera. For this reason, it was positioned so that the entire target would enter the lens and as far away from the backdrop, close to the camera as possible in Figure 3.8.

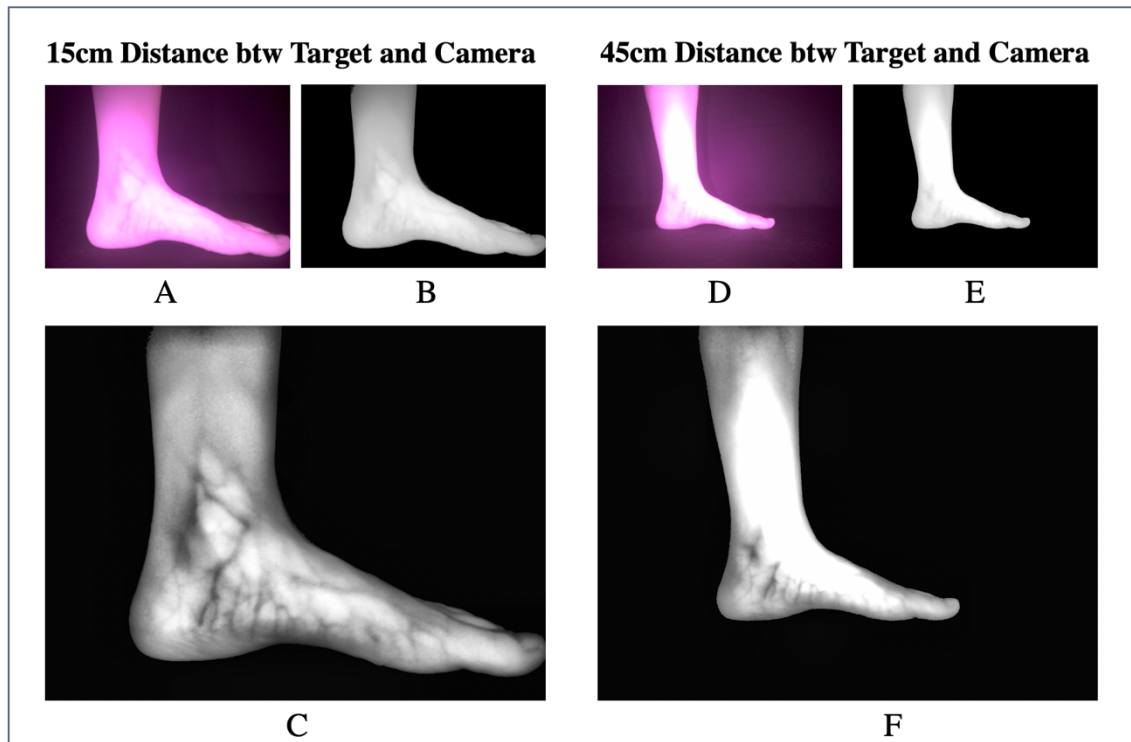


Figure 3.8. Images captured by changing the distance of the target to the camera. Glare and data loss increase as you move closer to the target backdrop and away from the camera.

3.2.3. Imaging Vascular Structures in Different Parts of the Body (Hand and Arm)

In the system where we made all the adjustment, tests were made on the hand and arm images. According to the results obtained, it has been found that the device is also effective in visualizing the surface vascular structures in different parts of the body (Figure 3.9).

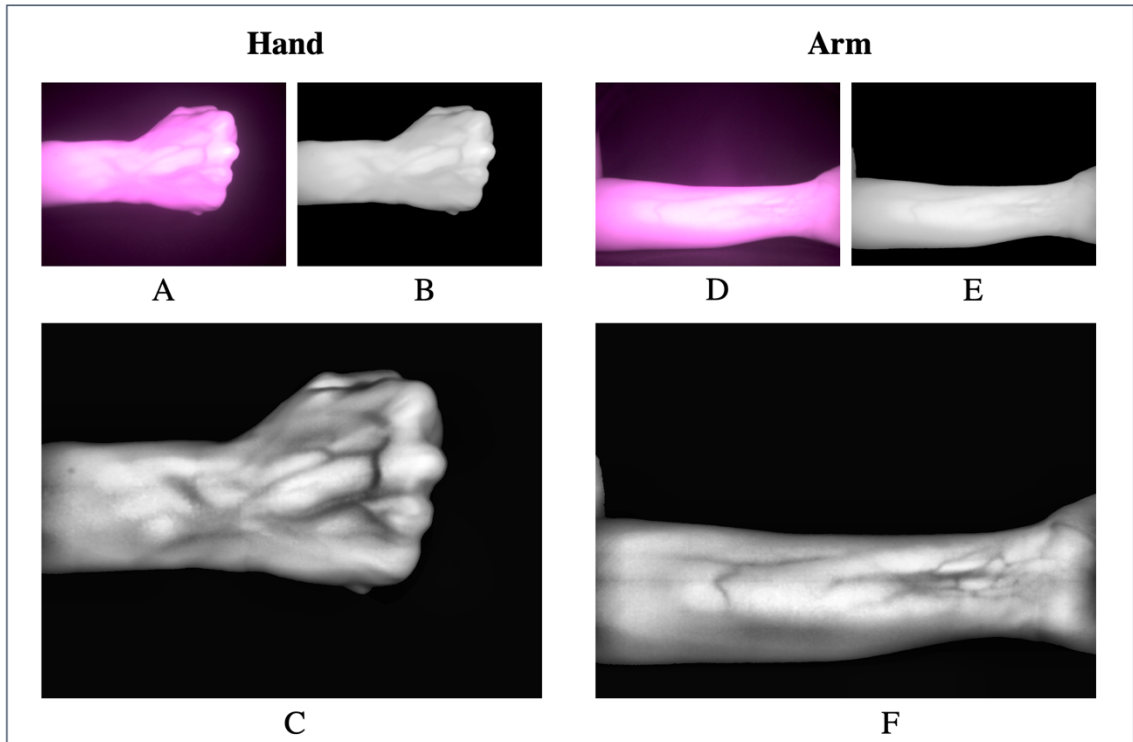


Figure 3.9. Hand and arm images captured after making adjustments to the device. (A, D) raw images, (B, E) images with removed background, (C, F) CLAHE applied.

3.3. Real-time Video Processing

The following section includes the real-time investigation vascular structures, which is the main purpose of our study.

First, we created frames and segmented the target from the background. For this, we converted the BGR image we obtained to HSV (hue, saturation, value). HSV represents the color space and is an effective model in segmentation processes in terms of dividing objects into sections according to their color. Then we converted the background cleared image from HSV to grayscale. The reason we do the operations in grayscale instead of BGR is to switch the image from 3D area (red, green, blue) to 2D (black and white) area, that is, to complete operations with smaller data in a shorter time. The CLAHE process was applied three times to further clarify the vascular image by increasing the contrast. Finally, median filter was applied on the image to eliminate factors that could cause noise such as hair on the target (Figure 3.10).

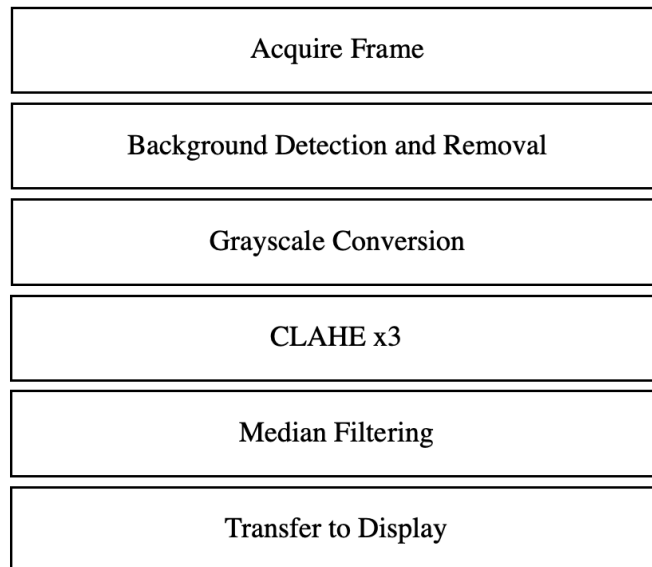


Figure 3.10. Block diagram of the real-time video processing.

In Figure 3.11, the instant vessels image of the monitor is shown and a screenshot of the real-time foot captured and processed on the monitor is given in Figure 3.12. The process is fast and the vascular structures is clearly visible.



Figure 3.11. Monitor screen showing the infrared image of a foot. The device is located next to the monitor.



Figure 3.12. A screenshot of the real-time foot image captured and processed on the monitor.

3.4. Image Processing

The improvement of the vascular images is an important procedure for clinical diagnosis. In addition to the real-time processing, we also tried to capture the vascular images as tube-like structures on the image. Unlike the methods we used in the previous section, we have added Frangi filter, which is a method applied in devices such as MRA, CTA, to this section. The Frangi filter offers higher edge contrast by making the vessel edges sharper [56]. The results of the procedure obtained images of the coronary arteries from X-ray angiography by using the Frangi filter to extract the coronary arteries in a study by Shashank et al. are shown in Figure 3.13.

In this study, the result of the operations performed Figure 3.14, the vessels were obtained tube-like structure. The results we obtained by using the Frangi filter are given in Figure 3.15. However, this method is not suitable for real-time processing as it extends the analysis time (approximately 3 minutes).

X-Ray Angiography Coronary Artery Images and Segmentation using Frangi Filter

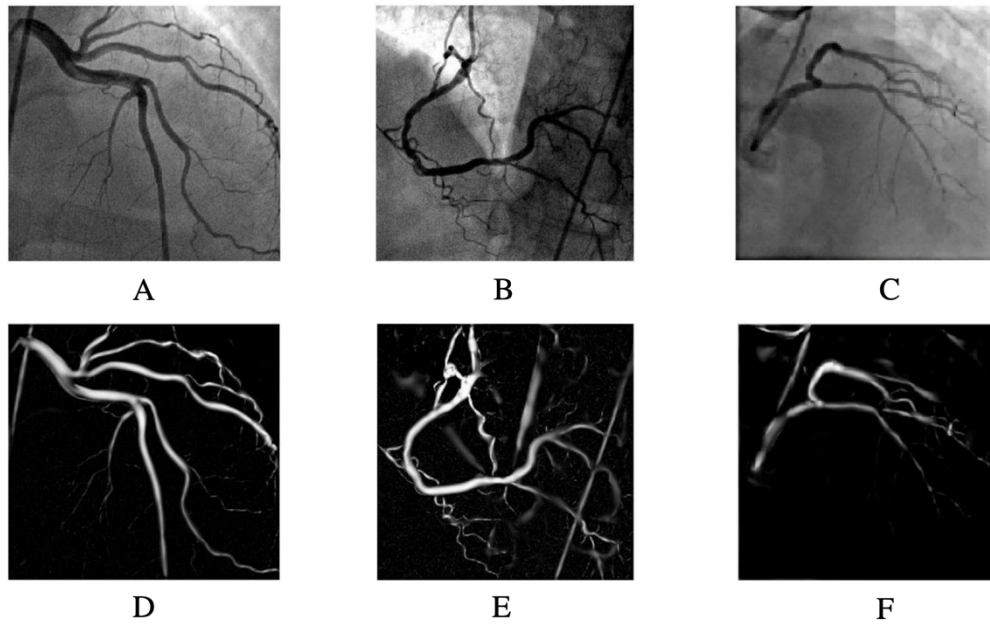


Figure 3.13. Coronary artery images obtained by X-ray angiography after enhanced with Frangi filter [57].

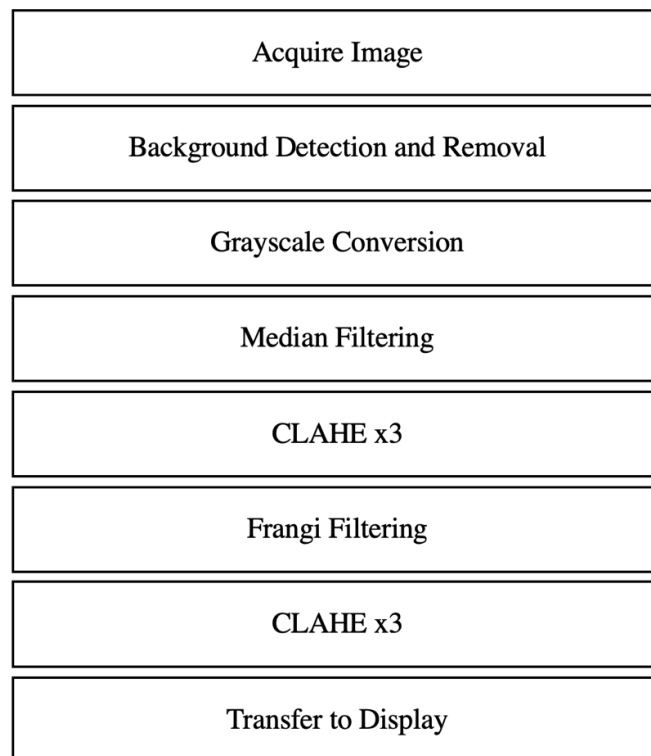


Figure 3.14. Block diagram of the image processing.

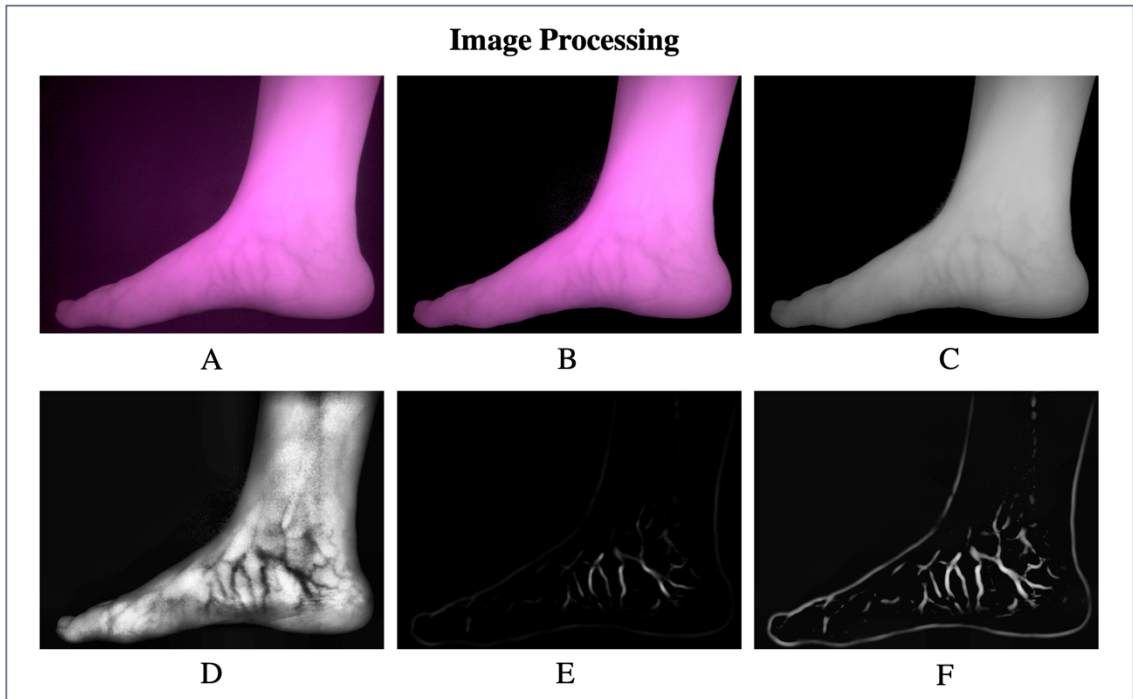


Figure 3.15. Image processing *(A)* raw image, *(B)* images with removed background, *(C)* grayscale conversion *(D)* 3 times CLAHE applied *(E)* Frangi filtering applied *(F)* 3 times CLAHE applied again.

The median filter effect was not understood because there was no noise like hair in the images we took. The grayscale and median filtering gave similar results. Therefore, the median filter result is not available in Figure 3.15.

3.5. Analysis of Images Captured from Volunteers

In this section, the analysis of instant vascular images captured from the participants will be examined in Figure 3.16, Figure 3.17, Figure 3.18, Figure 3.19, Figure 3.20, Figure 3.21, Figure 3.22. There were 5 volunteer participants. There are 3 people in different stages of diabetes, and 2 healthy people. Patient I is diabetic and has had toe amputation due to the diabetic foot. Patient II has diabetes and is using insulin. Patient III were not diagnosed with diabetes by a specialist. However, for the last 1 month, blood sugar values have been at the same level as diabetes patients. Healthy I and healthy II

people do not have diabetes. As a result of the controls, no abnormality was observed in the blood glucose values of the healthy individuals.

The captured images with our device from diabetes and healthy people and their results were compared. Circulation disorders were detected in the images captured, the reason may not only diabetes, but also different diseases, unhealthy nutrition, inactivity, etc. For an accurate interpretation, it needs to be reviewed by an expert. Examination of the images captured at this stage over a period of time will make the result of the study more meaningful since it might enable the analysis of the disease progression over time.

The circulatory system carries nutrients and oxygen to the extremum points of the body and at the same time ensures the return of dirty blood to the heart. Blood circulation disorder causes disruption of this conduction system and also causes many diseases affecting all organs and systems such as anemia, late healing of wounds, ulcers etc. Early detection of abnormalities in the blood circulation has an important role in treatments and at the same time contributes to the patient's awareness of healthy nutrition, clothing selection, stress management and exercise. With this device, we aimed to help early notice of negative situations that may be caused by circulatory disorders and to raise awareness for people who have unexpected blood vessel images to take precautions. Moreover, it is thought that the superficial vessel images captured with this device will help to observe the effect of varicose veins treatment in plastic surgery and to control whether the disease progresses or recurs.

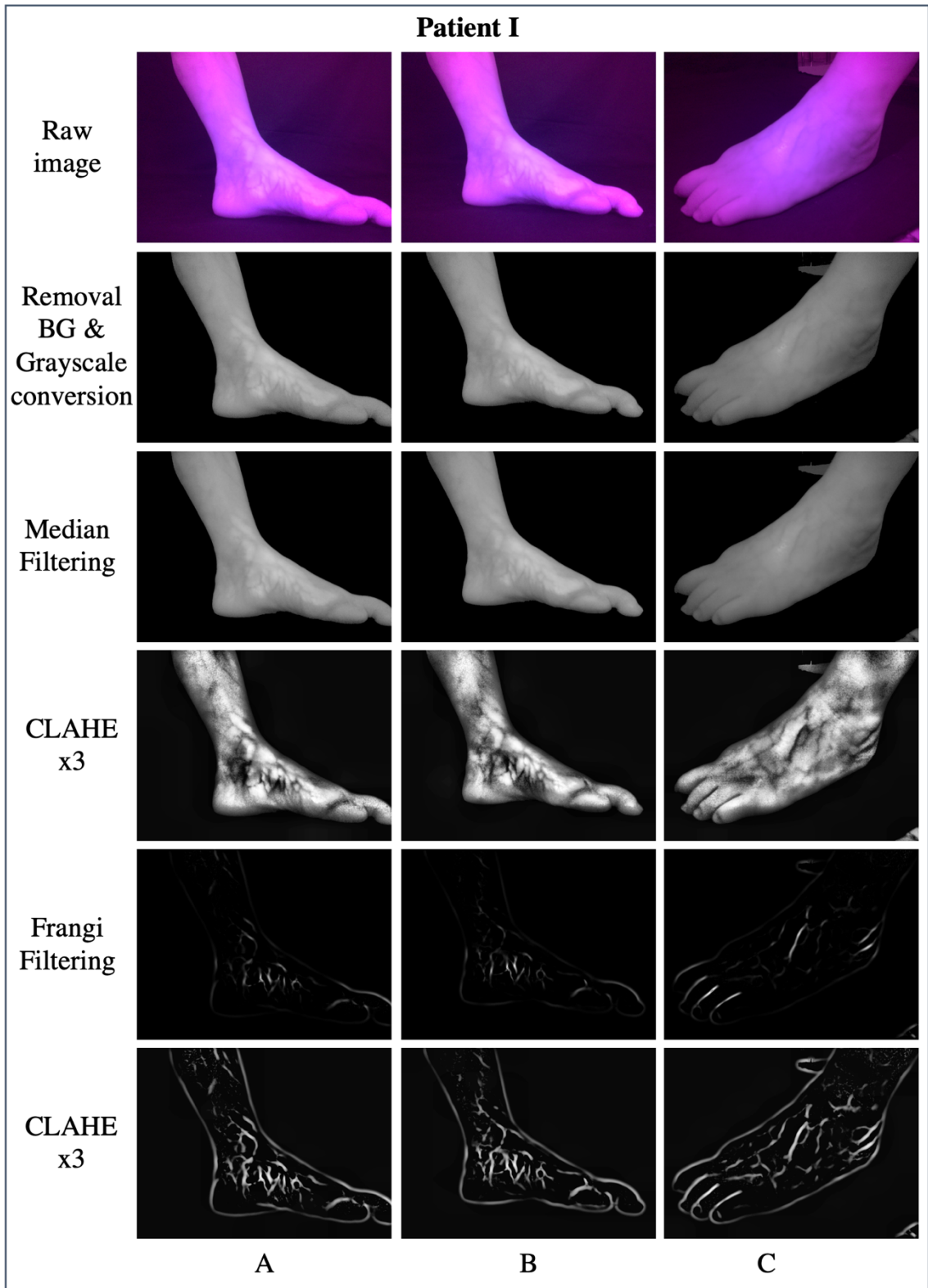


Figure 3.16. Image processing applied to foot images of elderly diabetic person “Patient I” with toe amputation due to diabetic foot.

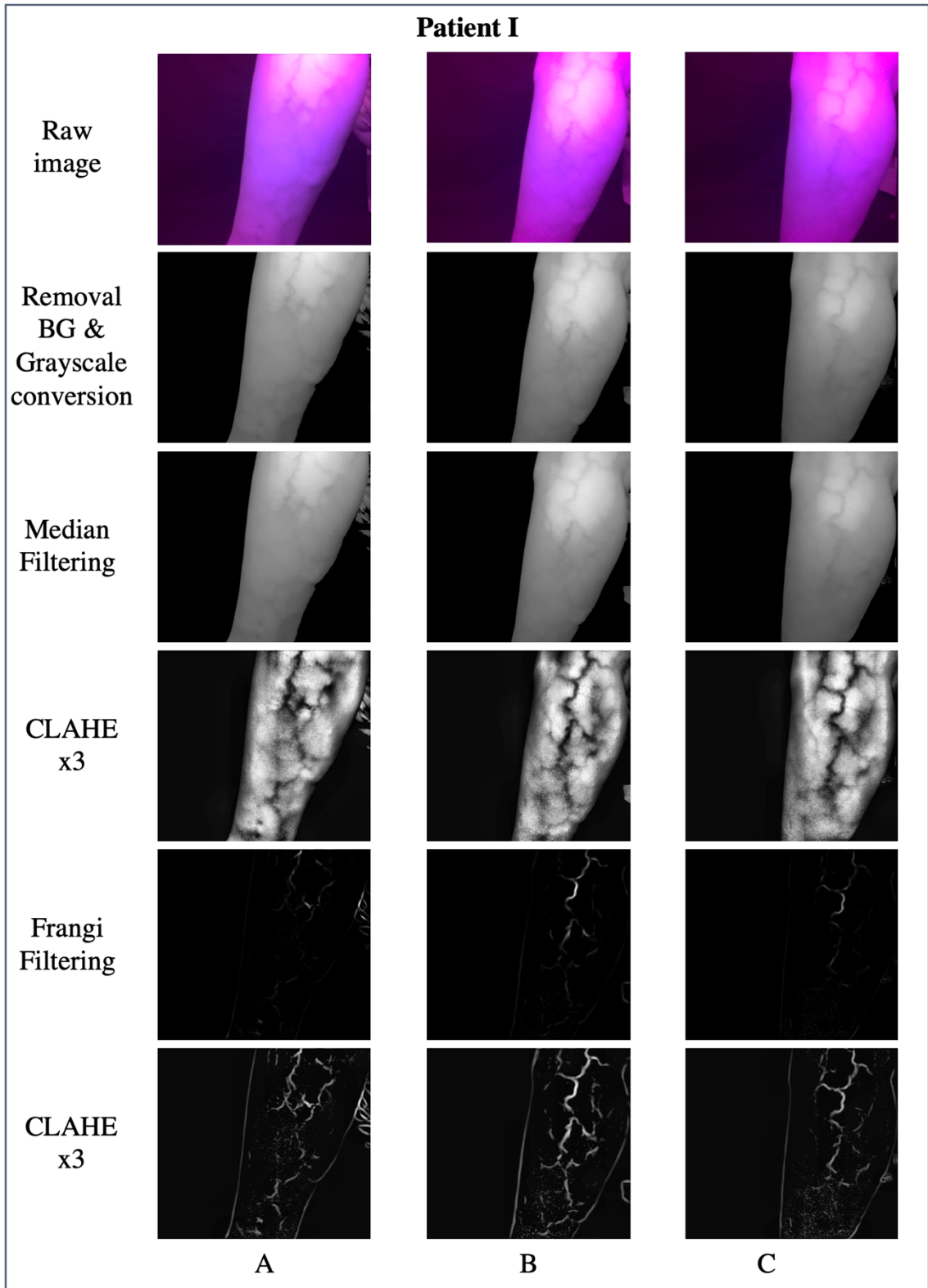


Figure 3.17. Vascular structures of the elderly diabetic person with the diabetic foot (Patient I) in Figure 3.16.

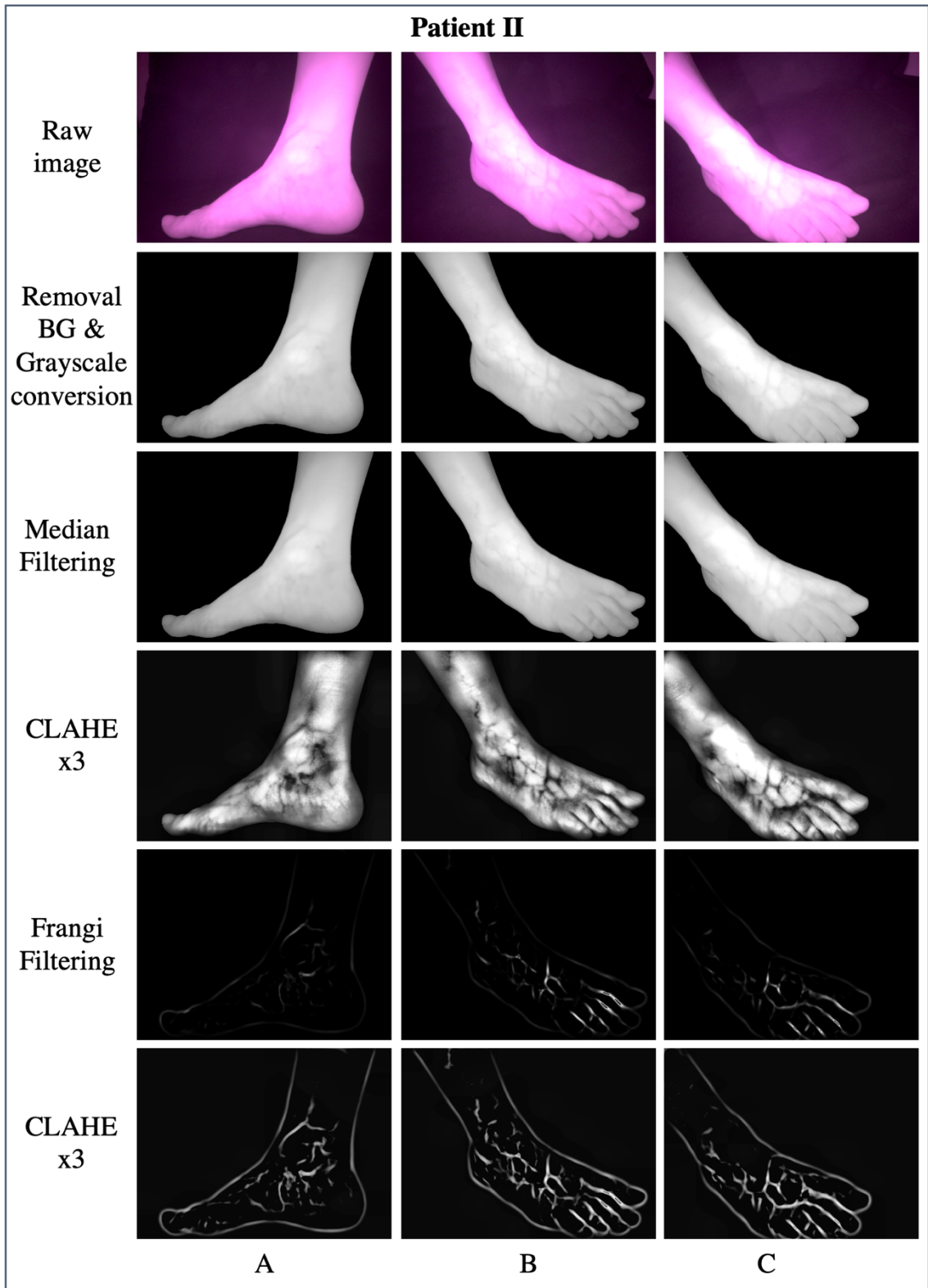


Figure 3.18. Image processing applied to foot of a middle-aged person (Patient II) with diabetes using insulin.

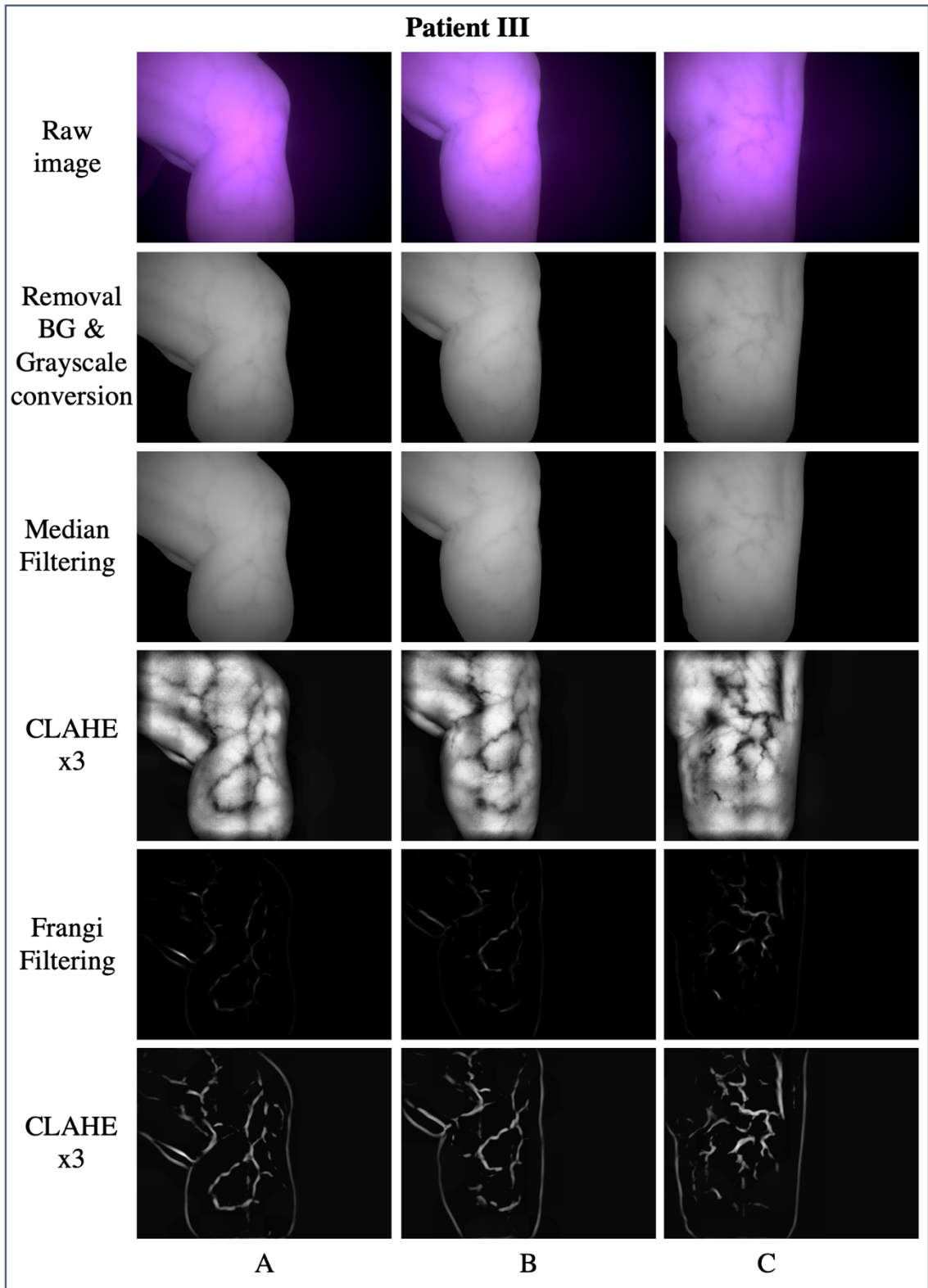


Figure 3.19. Vascular structures of a middle-aged person (Patient III) who has not had diabetes but has high blood sugar levels for the last 1 month and also has varicose veins.

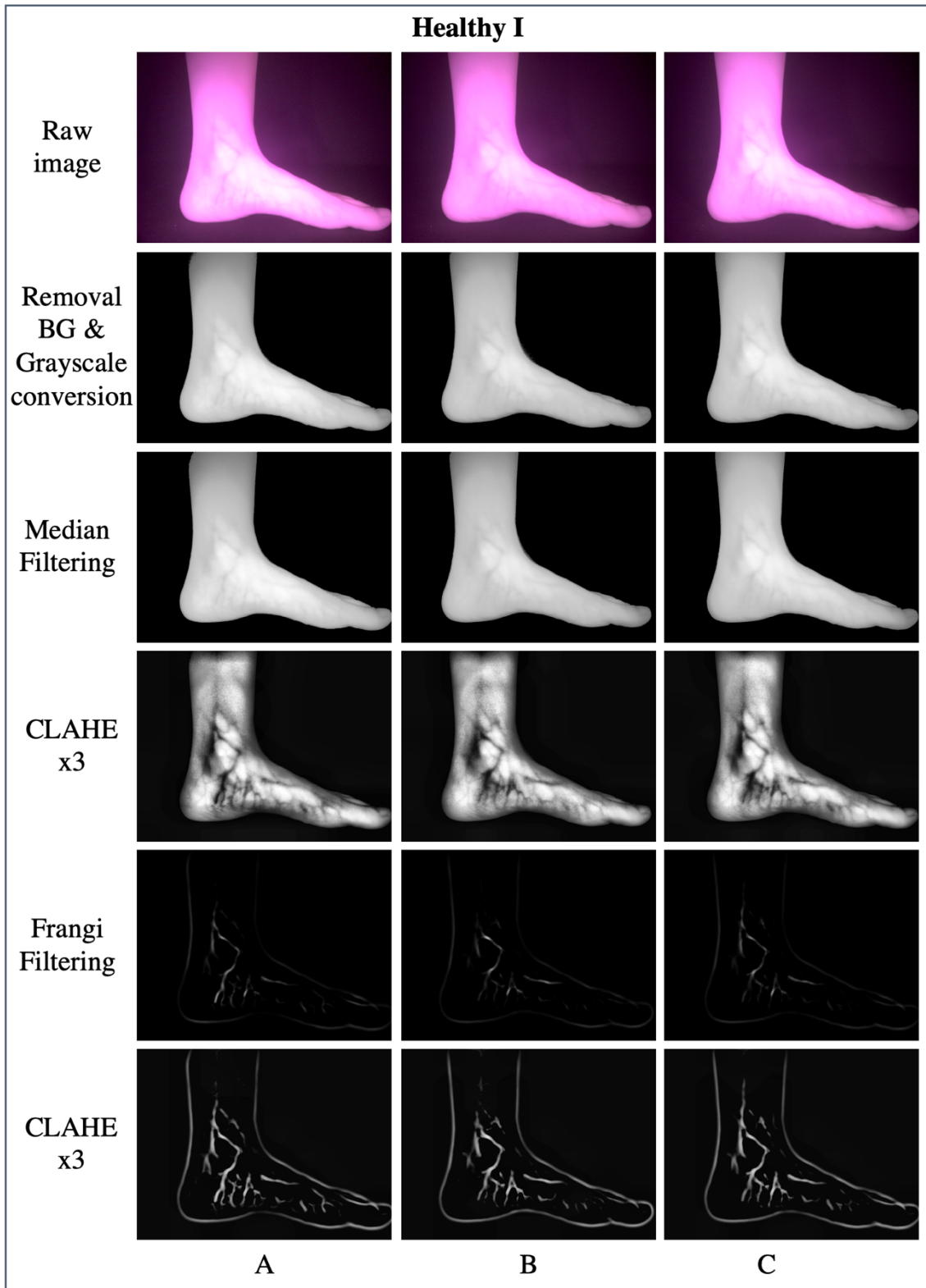


Figure 3.20. Image processing applied to foot of a healthy young person (Healthy I).

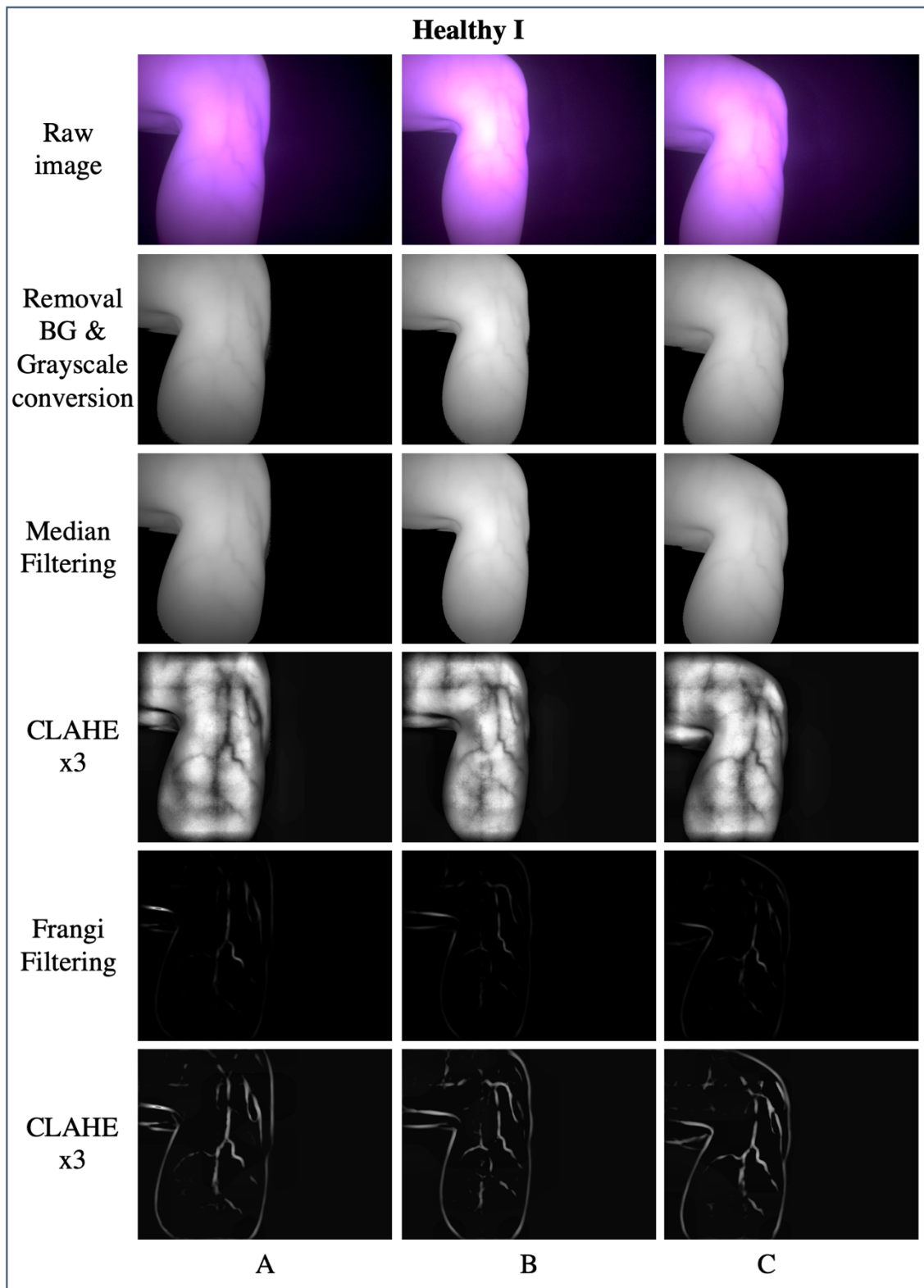


Figure 3.21. The vascular structures of a healthy young person (Healthy I) who does not show any visible abnormality.

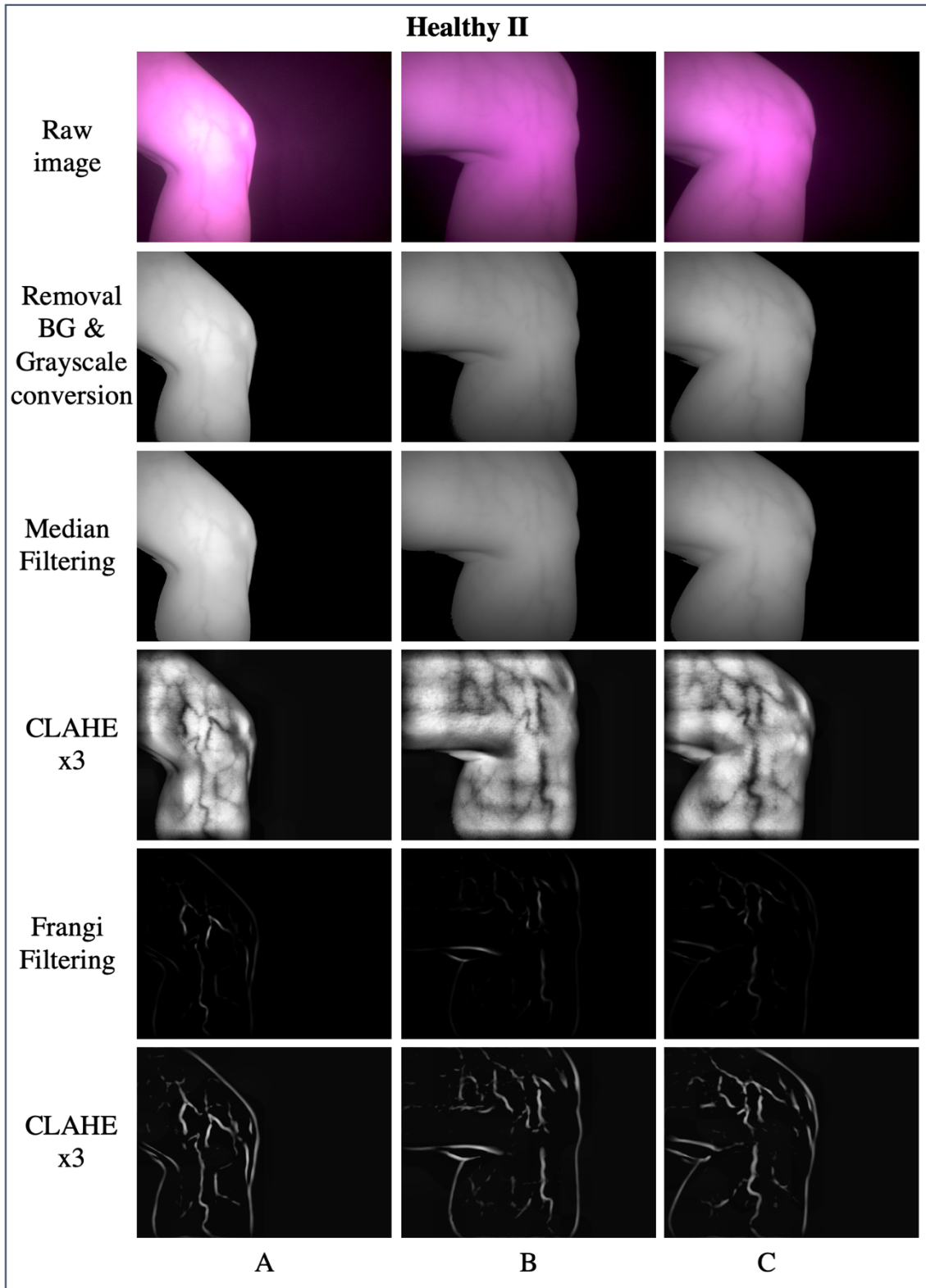


Figure 3.22. The vascular structures in a young person (Healthy II) who does not have diabetes.

CHAPTER 4

CONCLUSIONS

Using commercially available electronic and optical components, we developed a real-time, non-contact and safe vascular imaging system at low-cost for early diagnosis of abnormalities in the superficial vessel structures. Compared to the advanced medical imaging techniques, our system has advantages in terms of cost, size and safety.

Hardware design consist of two 850 nm NIR LEDs reflecting at a right angle to the target, a filter eliminating the ambient light and diffusers that scatter the light from the LEDs for capturing superficial blood vessels in daylight. A black backdrop was used in the background to easily remove the target while capturing pictures and video frames. The cost of the system design, including all materials used for tests and computer monitor, did not exceed 5.000 Turkish liras (~600 U.S. dollars).

System software consists of two parts: one for real-time video processing and the other for image processing. The video processing algorithm was tested on captured foot images from the device using a fast algorithm suitable for real-time processing. The image process part uses Frangi filter, which is applied in angiography imaging devices to obtain vessels as tubular structure. However, due to the long processing time (~3 min.), it was not suitable for real-time video processing.

After optimizing the optimal viewing conditions and software, the images were collected from diabetes (Patient I, II, III) and healthy (Healthy I, II) people. The captured images from people with diabetes exhibited abnormalities in the vascular structures compared to the images captured from the healthy people. In order to understand the effectiveness and accuracy of the device, vessel images can be viewed for a certain period of time and results obtained with the device can be compared with angiography images.

This study has been designed for the early diagnosis of abnormalities in the vascular structures. It is also expected to assist health professionals to monitor how the patient responds to the treatments of vascular diseases by comparing the images captured at different times during the treatments.

REFERENCES

- [1] R. Goldman, C. S. Harbor, O. Rourke, and S. E. A. E, “US8463364,” vol. 2, no. 12, 2013.
- [2] C. M. Kramer *et al.*, “ACCF/AHA 2007 Clinical Competence Statement on Vascular Imaging With Computed Tomography and Magnetic Resonance.,” *J. Am. Coll. Cardiol.*, vol. 50, no. 11, pp. 1097–1114, 2007, doi: 10.1016/j.jacc.2007.07.006.
- [3] J. W. Norris and A. Halliday, “Is Ultrasound Sufficient for Vascular Imaging Prior to Carotid Endarterectomy?,” *Stroke*, vol. 35, no. 2, pp. 370–371, 2004, doi: 10.1161/01.STR.0000115295.63866.E0.
- [4] B. M. Dale, M. A. Brown, and R. C. Semelka, *MRI Basic Principles and Applications*. Chichester, UK: John Wiley & Sons, Ltd, 2015.
- [5] R. W. van Hamersvelt *et al.*, “Contrast agent concentration optimization in CTA using low tube voltage and dual-energy CT in multiple vendors: a phantom study,” *Int. J. Cardiovasc. Imaging*, vol. 34, no. 8, pp. 1265–1275, 2018, doi: 10.1007/s10554-018-1329-x.
- [6] M. Goyen, S. G. Ruehm, and J. F. Debatin, “MR-angiography: The role of contrast agents,” *Eur. J. Radiol.*, vol. 34, no. 3, pp. 247–256, 2000, doi: 10.1016/S0720-048X(00)00203-5.
- [7] D. Ai *et al.*, “Augmented reality based real-time subcutaneous vein imaging system,” vol. 7, no. 7, pp. 39–49, 2016, doi: 10.1364/BOE.7.002565.
- [8] B. D. Alessandro and A. P. Dhawan, “Transillumination Imaging for Blood Oxygen Saturation Estimation of Skin Lesions,” vol. 59, no. 9, pp. 2660–2667, 2012.
- [9] D. Huang, X. Zhu, Y. Wang, and D. Zhang, “Dorsal hand vein recognition via hierarchical combination of texture and shape clues,” *Neurocomputing*, vol. 214, pp. 815–828, 2016, doi: 10.1016/j.neucom.2016.06.057.
- [10] D. Huang, R. Zhang, Y. Yin, Y. Wang, and Y. Wang, “Local feature approach to dorsal hand vein recognition by Centroid-based Circular Key-point Grid and fine-grained matching,” *Image Vis. Comput.*, vol. 58, pp. 266–277, 2017, doi: 10.1016/j.imavis.2016.07.001.
- [11] S. Barra, M. De Marsico, M. Nappi, F. Narducci, and D. Riccio, “A hand-based

- biometric system in visible light for mobile environments,” *Inf. Sci. (Ny)*., vol. 479, pp. 472–485, 2019, doi: 10.1016/j.ins.2018.01.010.
- [12] J. Wang and G. Wang, “Hand-dorsa vein recognition with structure growing guided CNN,” *Optik (Stuttg)*., vol. 149, pp. 469–477, 2017, doi: 10.1016/j.ijleo.2017.09.064.
- [13] J. Wang, G. Wang, M. Li, and W. Du, “Hand vein recognition based on PCET,” *Optik (Stuttg)*., vol. 127, no. 19, pp. 7663–7669, 2016, doi: 10.1016/j.ijleo.2016.05.119.
- [14] V. P. Zharov, S. Ferguson, J. F. Eidt, P. C. Howard, L. M. Fink, and M. Waner, “Infrared Imaging of Subcutaneous Veins,” *Lasers Surg. Med.*, vol. 34, no. 1, pp. 56–61, 2004, doi: 10.1002/lsm.10248.
- [15] O. Abdeladl, M. Schleicher, M. Portilla, A. Shaporev, and V. Reukov, “Development of a portable near infrared camera for early detection of diabetic ulcers,” *Proc. - 32nd South. Biomed. Eng. Conf. SBEC 2016*, pp. 55–56, 2016, doi: 10.1109/SBEC.2016.73.
- [16] I. D. F. D. Atlas, *463 PEOPLE LIVING WITH DIABETES million*. 2019.
- [17] K. M. Raspovic and D. K. Wukich, “Self-reported quality of life and diabetic foot infections,” *J. Foot Ankle Surg.*, vol. 53, no. 6, pp. 716–719, 2014, doi: 10.1053/j.jfas.2014.06.011.
- [18] S. M. Marshall and A. Flyvbjerg, “Prevention and early detection of vascular complications of diabetes,” *Br. Med. J.*, vol. 333, no. 7566, pp. 475–480, 2006, doi: 10.1136/bmj.38922.650521.80.
- [19] J. Apelqvist and J. Larsson, “What is the most effective way to reduce incidence of amputation in the diabetic foot?,” *Diabetes. Metab. Res. Rev.*, vol. 16, no. SUPPL. 1, 2000, doi: 10.1002/1520-7560(200009/10)16:1+<::AID-DMRR139>3.0.CO;2-8.
- [20] S. Beckert, M. Witte, C. Wicke, A. Königsrainer, and S. Coerper, “A new wound-based severity score for diabetic foot ulcers: A prospective analysis of 1,000 patients,” *Diabetes Care*, vol. 29, no. 5, pp. 988–992, 2006, doi: 10.2337/dc05-2431.
- [21] R. J. H. N. C. Schaper, G. Andros, J. Apelqvist, K. Bakker, J. Lammer, M. Lepantalo, J. L. Mills, J. Reekers, C. P. Shearman, R. E. Zierler, “Diagnosis and treatment of peripheral arterial disease in diabetic patients with a foot ulcer. A progress report of the International Working Group on the Diabetic Foot†,”

- Diabetes. Metab. Res. Rev.*, vol. 32, no. 30, pp. 13–23, 2014, doi: 10.1002/dmrr.
- [22] F. W. Commons, “File : Oxy and Deoxy Hemoglobin Near-Infrared absorption spectra . png,” no. August 2012.
- [23] D. Barolet, F. Christiaens, and M. R. Hamblin, “Infrared and skin: Friend or foe,” *J. Photochem. Photobiol. B Biol.*, vol. 155, no. December, pp. 78–85, 2016, doi: 10.1016/j.jphotobiol.2015.12.014.
- [24] F. Schiffer *et al.*, “Psychological benefits 2 and 4 weeks after a single treatment with near infrared light to the forehead: a pilot study of 10 patients with major depression and anxiety,” *Behav. Brain Funct.*, vol. 5, no. 1, p. 46, 2009, doi: 10.1186/1744-9081-5-46.
- [25] D. M. Johnstone, C. Moro, J. Stone, A. L. Benabid, and J. Mitrofanis, “Turning on lights to stop neurodegeneration: The potential of near infrared light therapy in Alzheimer’s and Parkinson’s Disease,” *Front. Neurosci.*, vol. 9, no. JAN, pp. 1–15, 2016, doi: 10.3389/fnins.2015.00500.
- [26] M. G. Sowa, W.-C. Kuo, A. C.-T. Ko, and D. G. Armstrong, “Review of near-infrared methods for wound assessment,” *J. Biomed. Opt.*, vol. 21, no. 9, p. 091304, 2016, doi: 10.1117/1.jbo.21.9.091304.
- [27] K. H. D. Nguyen, A. L. T. Nguyen, and H. T. T. Pham, “Constructing real time vein imaging device utilizing near infrared technology and embedded system,” *IFMBE Proc.*, vol. 63, pp. 559–562, 2018, doi: 10.1007/978-981-10-4361-1_95.
- [28] D. Ai *et al.*, “Augmented reality based real-time subcutaneous vein imaging system,” *Biomed. Opt. Express*, vol. 7, no. 7, p. 2565, 2016, doi: 10.1364/boe.7.002565.
- [29] H. D. Zeman and G. Lovhoiden, “Vein Imaging: A New Method of Near Infrared Imaging, Where a Processed Image Is Projected onto the Skin for the Enhancement of Vein Treatment,” pp. 1031–1038, 2006, doi: 10.1111/j.1524-4725.2006.32226.x.
- [30] D. Kim, Y. Kim, S. Yoon, and D. Lee, “Preliminary study for designing a novel vein-visualizing device,” *Sensors (Switzerland)*, vol. 17, no. 2, 2017, doi: 10.3390/s17020304.
- [31] N. J. Cuper *et al.*, “Medical Engineering & Physics The use of near-infrared light for safe and effective visualization of subsurface blood vessels to facilitate blood withdrawal in children,” *Med. Eng. Phys.*, vol. 35, no. 4, pp. 433–440, 2013, doi: 10.1016/j.medengphy.2012.06.007.

- [32] M. Engin and E. Engineering, “Deep tissue near-infrared imaging for vascular network analysis,” vol. 10, no. 3, pp. 1–12, 2017, doi: 10.1142/S1793545816500516.
- [33] H. Gudmann, S. Brandt, C. H. Jepsen, O. M. Hendriksen, A. Lindekær, and M. Skjønnemand, “The use of ultrasound to identify veins for peripheral venous access in morbidly obese patients,” no. February, pp. 2–5, 2016.
- [34] M. W. Wukitsch, M. T. Petterson, D. R. Tobler, and J. A. Pologe, “Pulse oximetry: Analysis of theory, technology, and practice,” *J. Clin. Monit.*, vol. 4, no. 4, pp. 290–301, 1988, doi: 10.1007/BF01617328.
- [35] J. Hashimoto, “Finger vein authentication technology and its future,” *IEEE Symp. VLSI Circuits, Dig. Tech. Pap.*, vol. 00, no. c, pp. 5–8, 2006, doi: 10.1109/vlsic.2006.1705285.
- [36] M. Z. Yildiz and Ö. F. Boyraz, “Development of a low-cost microcomputer based vein imaging system,” *Infrared Phys. Technol.*, vol. 98, no. March, pp. 27–35, 2019, doi: 10.1016/j.infrared.2019.02.010.
- [37] T. Ahmed *et al.*, “Real time injecting device with automated robust vein detection using near infrared camera and live video,” *GHTC 2017 - IEEE Glob. Humanit. Technol. Conf. Proc.*, vol. 2017-Janua, pp. 1–8, 2017, doi: 10.1109/GHTC.2017.8239298.
- [38] G. Kanimozhi and A. S. A. Khadir, “Cryptosystem Based On Finger Vein Patterns Using Vas Algorithm,” *Int. J. Sci. Technol. Res.*, vol. 5, no. 5, pp. 130–137, 2016.
- [39] G. Sakthivel, “Hand Vein Detection using Infrared Light for Web based Account,” *Int. J. Comput. Appl.*, vol. 112, no. 10, pp. 17–22, 2015.
- [40] S. Damavandinejadmonfared, “Finger vein recognition using linear kernel entropy component analysis,” *Proc. - 2012 IEEE 8th Int. Conf. Intell. Comput. Commun. Process. ICCP 2012*, pp. 249–252, 2012, doi: 10.1109/ICCP.2012.6356194.
- [41] Y. Wang, D. Wang, T. Liu, and X. Li, “Local SIFT analysis for hand vein pattern verification,” vol. 7512, pp. 1–8, 2009, doi: 10.1117/12.837104.
- [42] T. Yanagawa and T. Ohyama, “Human finger vein images are diverse and its patterns are useful for personal identification Faculty of Mathematics Kyushu University,” no. November 2014.
- [43] “Infographic Maker - Create Infographics Online | Mind the Graph.” .
- [44] “High Power LED Light Source Application & Solutions, TaoYuan LED.” .
- [45] “Teach, Learn, and Make with Raspberry Pi – Raspberry Pi.” .

- [46] “HOYA | The Difference is Clear.” .
- [47] “Flash-Lens-LED Light-Flash Trigger-TTL Remote Cord-Wireless Shutter Release-Flash Equipment - YONGNUO photographic equipment Co., Ltd.” .
- [48] “NVIDIA Jetson Nano Developer Kit | NVIDIA Developer.” .
- [49] C. Saravanan, “Color image to grayscale image conversion,” *2010 2nd Int. Conf. Comput. Eng. Appl. ICCEA 2010*, vol. 2, pp. 196–199, 2010, doi: 10.1109/ICCEA.2010.192.
- [50] S. Gupta and S. Singh, “Curvelet based Rayleigh CLAHE Medical Image Enhancement,” *Int. J. Comput. Appl.*, vol. 182, no. 6, pp. 19–23, 2018, doi: 10.5120/ijca2018917554.
- [51] A. M. Reza, “Realization of the contrast limited adaptive histogram equalization (CLAHE) for real-time image enhancement,” *J. VLSI Signal Process. Syst. Signal Image. Video Technol.*, vol. 38, no. 1, pp. 35–44, 2004, doi: 10.1023/B:VLSI.0000028532.53893.82.
- [52] Z. Al-Ameen, G. Sulong, A. Rehman, A. Al-Dhelaan, T. Saba, and M. Al-Rodhaan, “An innovative technique for contrast enhancement of computed tomography images using normalized gamma-corrected contrast-limited adaptive histogram equalization,” *EURASIP J. Adv. Signal Process.*, vol. 2015, no. 1, pp. 1–12, 2015, doi: 10.1186/s13634-015-0214-1.
- [53] A. F. Frangi, W. J. Niessen, K. L. Vincken, and M. A. Viergever, “Multiscale vessel enhancement filtering,” *Lect. Notes Comput. Sci. (including Subser. Lect. Notes Artif. Intell. Lect. Notes Bioinformatics)*, vol. 1496, pp. 130–137, 1998, doi: 10.1007/bfb0056195.
- [54] “Circuit Diagram - A Circuit Diagram Maker.” .
- [55] T. Kato, M. Kondo, K. Hattori, R. Taguchi, M. Hoguro, and T. Umezaki, “Development of penetrate and reflection type finger vein certification,” *2012 Int. Symp. Micro-NanoMechatronics Hum. Sci. MHS 2012*, pp. 501–506, 2012, doi: 10.1109/MHS.2012.6492503.
- [56] X. Xu, B. Liu, and F. Zhou, “Hessian-based Vessel Enhancement Combined with Directional Filter Banks and Vessel Similarity,” pp. 80–84, 2013.
- [57] M. Bhattacharya and G. K. Sharma, “Optimized Coronary Artery Segmentation Using Frangi Filter and Anisotropic Diffusion Filtering Optimized Coronary Artery Segmentation using Frangi filter and Anisotropic Diffusion Filtering,” no. August, 2013, doi: 10.1109/ISCBI.2013.59.

